Design of Intestine Inspection Device

Anand Sekar

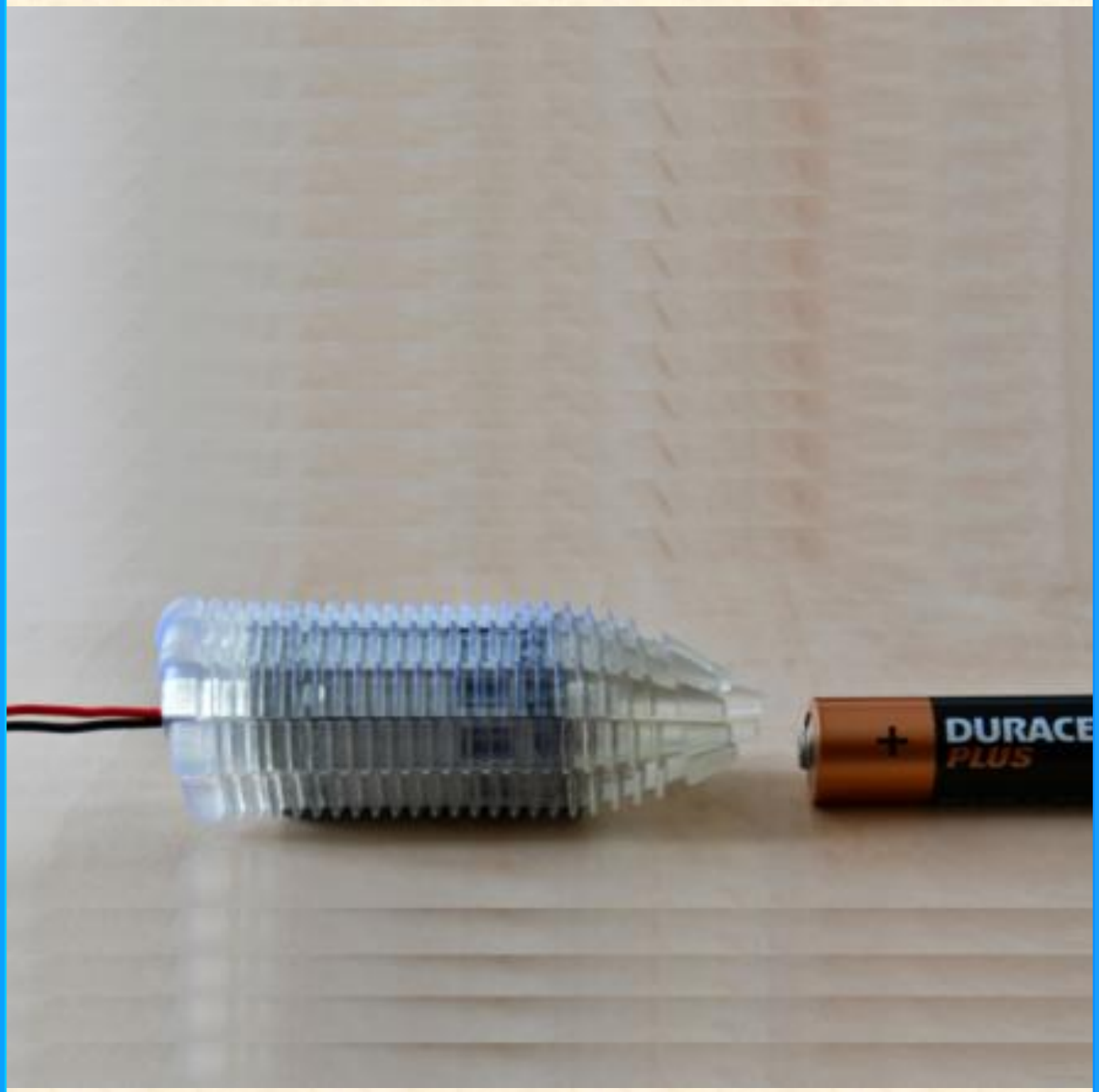

Supervisors: Paul Breedveld

Mostafa Atalla

TU Delft Delft University of Technology

Challenge the future

Technische Universiteit Delft

Design of Intestine Inspection Device

by

Anand Sekar

A thesis presented for the degree of Master of Science
in Mechanical Engineering (Biomechanical Design track)

Delft University of Technology
To be defended on 8 August 2023 at 09:45

Student number:	5285119	
Thesis committee:	Paul Breedveld,	Supervisor
	Aimée Sakes	
	Mostafa Atalla,	Daily supervisor

TU Delft Delft University of Technology

CONTENTS

I Introduction 2

II Design requirements 3

III Concept design 4
III-A From earthworm to ovipositor design . . . 4
III-B Actuation system design . . . 5
III-C Friction surface design . . . 6

IV Detailed design 6
IV-A Slider unit design . . . 7
IV-B Cam design . . . 8
IV-C Motor & frame design . . . 9
IV-D Prototype development . . . 9

V Experiment 10
V-A Construction of experiment set-up . . . 10
V-B Experimental procedure . . . 11
V-C Results . . . 11

VI Discussion & Future research 12

VII Conclusion 13

References 13

Appendix A: Calculation for determining maximum number of sliders 15

Appendix B: Motor force derivation 15

Appendix C: Motor torque calculation 16

Appendix D: Design drawings 16

Design of Intestine Inspection Device

Anand Sekar

***Abstract*—Colonoscopy is a widely used endoscopic procedure to diagnose colorectal cancer (CRC) which is considered the fourth most common cancer in the US and the second most common cancer in Europe. Colonoscope, used in colonoscopy, consists of a thin flexible hollow tube that is inserted into the rectum of a person and propagated through the entire colon. The disadvantage of the current procedure is that the colonoscope has to be pushed from outside to move through the colon resulting in recurrent looping of the colonoscope due to buckling. Recurrent looping inflicts the risk of tissue damage and is responsible for approximately 90% of the pain experienced by patients during colonoscopy. Research was carried out to create self-propelling colonoscopes which would eliminate the force required to push the device from outside. Inspirations were taken from the locomotion of earthworms to develop self-propelling colonoscopes however, the device's propulsion was hindered due to friction and low axial stiffness of the colon wall. In this study, a proof of concept for a self-propelled colonoscopic device inspired by the ovipositor of wasps was conducted which resulted in the development of a prototype. The prototype was tested in a colon-simulated environment and it was able to successfully propel through the prepared colon phantom after an initial manual run through the colon phantom. The requirement of an initial manual run was speculated to be due to the capillary adhesion and uneven oil spread in the colon phantom. The device had an average velocity of around 5.68 mm /s inside the colon phantom with an average efficiency of 72.5%. In the future, the prototype has to be tested in an actual colon to assess its functionality and evaluate the propulsion efficiency of the prototype in a real colon.**

***Index Terms*—Colon, Ovipositor, Self-propelling, Bio-inspired, Friction**

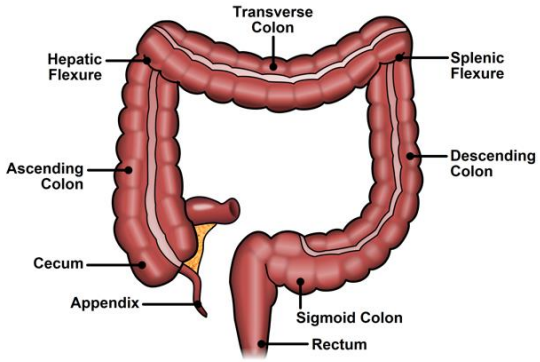

Fig. 1: Human colon [9]

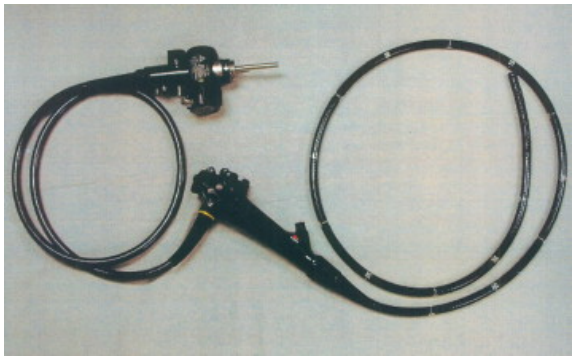

Fig. 2: Colonoscope [10]

I. Introduction

Colonoscopy is a widely used endoscopic procedure employed for the diagnosis and treatment of various conditions within the colon. It serves as an essential tool for detecting and managing colorectal cancer (CRC), polyps, bleeding, iron deficiency anemia, inflammatory bowel disease, and post-polypectomy and post-cancer resection surveillance [1], [2]. In the United States, colonoscopy is the most commonly utilized method for CRC detection, with more than 53% of the population undergoing this examination in 2012 [3]. Colorectal cancer ranks fourth among the most prevalent cancers in the US and second in Europe, and is the fourth leading cause of cancer-related deaths in the US [4], [5]. In Europe, colorectal cancer is the second leading cause of death among men and the third among women [6].

Colonoscopes are the devices used during colonoscopy to examine the colon that resembles a curved tube with segmented structures and bulges. Figure 1 provides a visual representation of the human colon and figure 2 depicts the conventional colonoscope that is in practice. The colonoscope consists of a thin, flexible, hollow tube that is inserted into the rectum and advanced to the cecum to diagnose and treat colon-related issues. With a length ranging from 160-180 cm (1.6-1.8 m), the colonoscope's flexibility enables gastroenterologists to navigate through the complex structure of the colon. Colonoscopes are equipped with LEDs and a camera at their front end to facilitate visual examination of the colon, along with two additional small channels that allow the passage of irrigants and instruments [7], [8].

Despite the widespread use of colonoscopy, certain disadvantages are hindering its acceptance rate among individuals. Some of the problems in colonoscopy include intestinal perforation, bleeding, and infections [11]. The colonoscope, during colonoscopy, requires an external push to advance inside the colon resulting in the buckling of the colonoscope. Buckling increases the external force required for device advancement and also gives rise to recurrent looping. Recurrent looping complicates the colonoscopic procedure by increasing the risk of tissue damage as well as compromising the visual clarity within the colon and is responsible for approximately 90% of the pain experienced by patients during colonoscopy. Consequently, these complications pose challenges to colonoscopic examinations, necessitating extensive operator training to ensure proficiency [12]–[14].

To address the buckling issue in colonoscopy, the concept of self-propelling colonoscopes has been proposed. Various mechanisms have been suggested, including replicating paddling motion, incorporating drive wheels for forward or backward movement, and utilizing momentum transfer for propulsion [12], [15], [16]. Mosse et al. conducted a study investigating the use of electrical stimulation for the propulsion through contraction of the colon wall. An oval-shaped device was equipped with four electrodes, positioned both at the front and back. By selectively applying a voltage to the front or back electrodes, the device can be propelled forward or backward, respectively [17], [18].

There were ideas of self-propelling colonoscopes that are pneumatically/hydraulically controlled . In a study, a folded sleeve was attached to the tip of the colonoscope that unfolds upon inflation, driving the tip forward. Additionally, the tip section includes a bendable region to facilitate navigation through the complex colon structure [19]. Similar research was carried out by Dehghani et al where the propulsion of the tip was facilitated by the unwinding of a coiled tube with the help of pneumatics [13]. In a study conducted by Pfeffer, propulsion using pressure difference was analysed by inflating a balloon inside the colon and infusing CO2 gas below or above the balloon to create a pressure difference [20]. Using hydraulics, Coleman et al conducted a study to propel a colonoscope where the colon was filled with water and the tip of the colonoscope consists of a capsule with nozzles around them. By adjusting the water pressure across the nozzles the propulsion inside the colon is achieved [21]. Actuation of self-propelling colonoscopes using magnets was researched by incorporating a permanent magnet within the device and utilizing an external magnetic field to control the motion of the device. Robotic arms were employed to manipulate the magnetic field, enabling external control of device motion inside the colon. However, the drawbacks of external control involve the need for sufficient space and the cost to set up an external magnetic field operated by a robotic arm [22].

Several self-propelling concepts were researched inspired by the earthworm. A study by Li et al developed a concept mimicking the swaying movement of the Cilia present in earthworms for propulsion [23]. Inspirations were also taken from the peristaltic locomotion of earthworms. The body of the earthworm consists of circular and longitudinal muscles as well as hairs called setae. Setae act as an anchor for the body and earthworm locomotes by alternatively contracting the circular and longitudinal muscles. To move forward, the front section of the body is anchored to the ground with the help of setae. Then, the longitudinal muscles contract, causing the body length to shorten. Subsequently, the back section of the body is anchored, the front section is released and the circular muscle contracts. This contraction increases the length of the body making the earthworm move forward. The cycle is repeated continuously to achieve locomotion [24]. Devices inspired by earthworm locomotion typically consist of an anchoring part that clamps onto the intestinal wall and a contracting/elongating part to propel. Research was carried out to develop various anchoring and contracting/elongating mechanisms [25]–[29].

The objective of this study is to present a proof of concept for a self-propelled colonoscopic device inspired by the ovipositor of wasps. The proposed device is evaluated in a simulated environment closely resembling the human colon. Through this research, we aim to contribute to the advancement of self-propulsion technology for colonoscopy, ultimately improving the patient experience and facilitating accurate diagnosis and treatment. This paper is structured as follows: Section II provides the requirements of the design, followed by concept design and detailed design in section III and IV respectively. The experimentation part of the study and the corresponding results are elaborated in section VI along with discussion and future research in section VII. Finally, a conclusion summarising the whole work is elucidated.

II. Design requirements

The device was developed with the help of certain requirements explained in the table I . A simple illustration of the device based on the given requirements can be visualised in figure 3.

TABLE I: Design Requirements

Name	Requirement	Description
Diameter	Max. 3 cm	The diameter of the human colon varies from each individual and also varies along different sections of the colon within a single individual. According to Stauffer and Pfeifer, as a general rule of thumb, the diameter of the cecum, transverse colon and descending colon are considered as 9 cm, 6 cm and 3 cm respectively [30]. The maximum diameter of 3 cm was chosen to prevent the colon from stretching which would induce pain to the patients and at the same time the available space for the components in the device is maximized
Length	Min. 3 cm	The minimum length of the device was chosen to be greater than the diameter of the device to ensure the device does not topple over during the propulsion
Shape	Inverse parabolic with less steep at the front and more steep at the back of the device	During the colonoscopy, the colon that is examined remains empty and closed. The inverse parabolic shape of the device helps to open the colon with ease and prevents damage infliction on the colon while opening.
Cross-section	Circular	The cross-section of the device was made to be circular to match it with that of the colon, utilizing the maximum available space inside the colon. Additionally, the circular cross-section enables uniform stress across its section and prevents the colon from getting damaged due to sharp edges.
Speed	Min. 1.7mm/s	The average length of the colon is about 150 cm long [31]. The time that would take to advance the conventional colonoscope till the end of the colon is around 15 minutes [32]. Thus, the device that is designed would require to travel at least a speed of 1.7 mm/s to be comparable with the conventional colonoscope.

Damage observation	Visual	The damage on the colon phantom during the propulsion of the device is visually observed.
Propulsion direction	Forward motion	The device was designed to have only one direction of propulsion inside the colon i.e. it can only be pushed into the colon. When the device is pushed into the colon, it is subjected to compression which causes buckling. However, pulling the device out of the colon does not face this issue as the device would be subjected to tension.

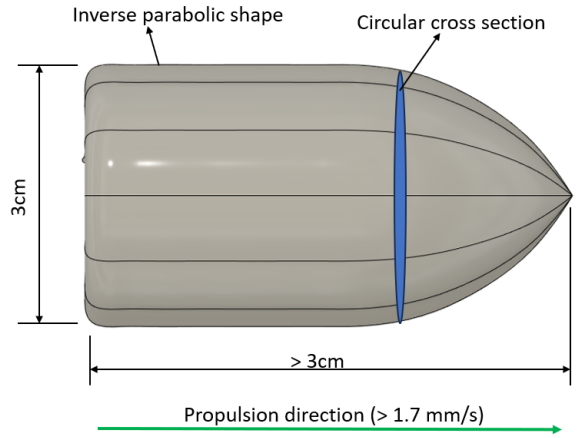

Fig. 3: Schematic representation of design requirements

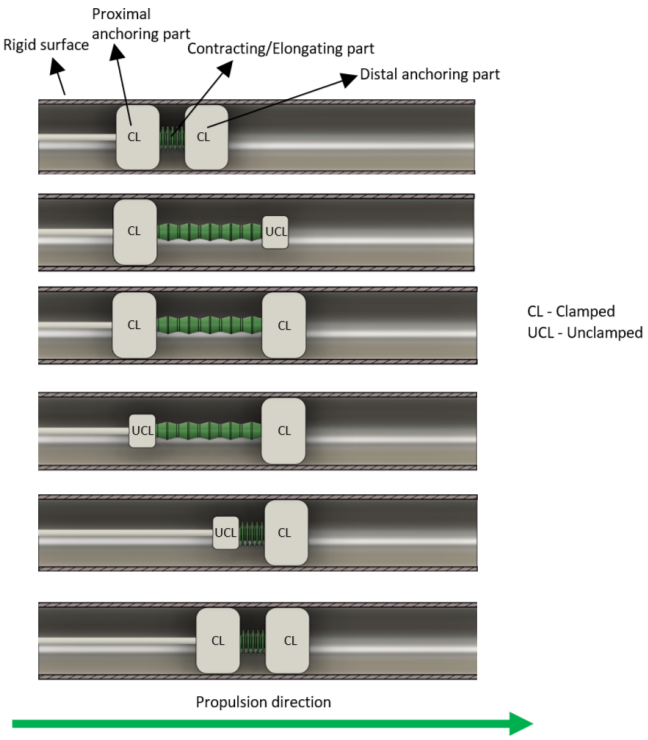

Fig. 4: Schematic representation of earthworm inspired locomotion

III. Concept design

A. From earthworm to ovipositor design

The systems inspired by the locomotion of earthworm has some disadvantages while propelling through the colon. Typically, the devices inspired by earthworm locomotion consist of a minimum of two anchoring parts and a contracting/elongating part. A simple illustration of the working mechanism of earthworm-inspired devices can be observed in figure 4. The propulsion using anchoring and sliding motion is hindered inside the colon due to friction and lower axial stiffness of the colon. The colon is subjected to intra-abdominal pressure leaving the colon in a closed state and the colon wall wraps around the surface of the device during propelling. When the proximal or distal anchoring part tries to move forward or backward, stretching or buckling of the colon wall occurs due to its friction and lower axial stiffness, impeding the device's propulsion [33]. A schematic representation of the propulsion of earthworm inspired devices causing the colon to stretch and buckle can be visualised in figure 5. This issue can be resolved by taking inspiration from the movement of the wasp's ovipositor. Unlike earthworm-inspired devices where the anchoring and sliding occur on different planes, the motion of the ovipositor incorporates anchoring and sliding elements on the same plane. This arrangement can resolve the stretching and buckling challenges encountered in earthworm-inspired devices.

Parasitic wasp uses an ovipositor to lay eggs by penetrating inside a solid/living substrate such as a tree or caterpillar. An ovipositor is a thin slender rod composed of four elements called valves, two on the ventral side and two on the dorsal

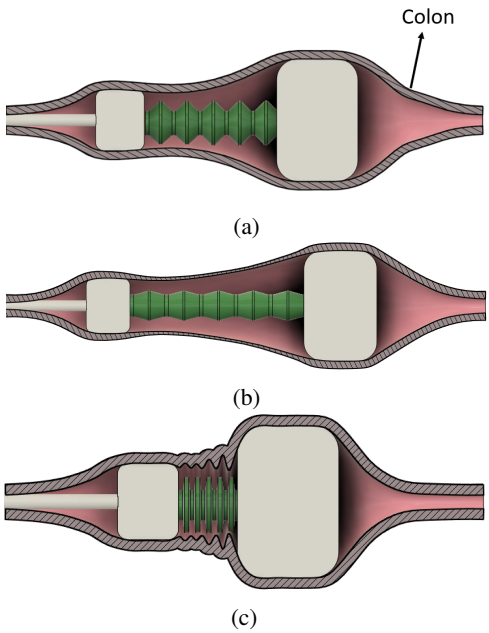

Fig. 5: Locomotion of eathworm inspired devices in a colon, a. when colon is in neutral position, b. when the colon is stretched, c. when the colon is buckled

side. However, the valves on the dorsal side are often merged due to the evolution thus making the total functional valve in the ovipositor to be three. The valves are capable of sliding along each other and are held together by a tongue and groove mechanism called olistheter. The ovipositor of a wasp can be visualised in figure 6. As ovipositors penetrate

inside a substrate to deposit eggs, there is a high chance for the ovipositor to get damaged from buckling. However, the ovipositor prevents buckling by strategically moving the valves with the help of friction and tension. At a time only one of the three valves is pushed some distance into the substrate while the other two valves remain stationary. The friction force of the stationary valves is higher than the friction force of the forward-moving valve. Additionally, the tension in the stationary valve is increased by pulling them back and serration at the tip of the valve prevents the stationary valves from moving when they are pulled back. Thus, the friction force and the tension of the two stationary valves compensate for the dynamic friction and the forces at the tip of the moving valve preventing the ovipositor from buckling [34]–[36]. Therefore, by constantly pushing valves one by one, the ovipositor can penetrate into the desired location in the substrate without any damage on the ovipositor.

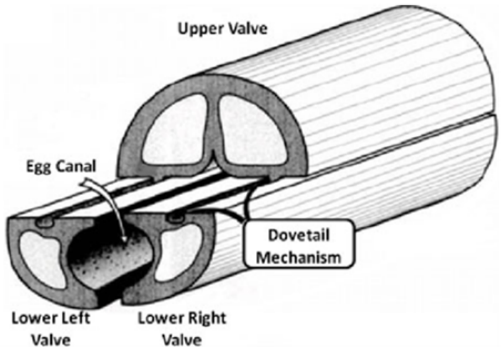

Fig. 6: Ovipositor of wasp [37]

The intestine inspection device consists of components similar to valves of the ovipositor that can translate back and forth. These would be referred to as sliders and are in contact with the walls of the colon during propulsion. Due to its contact, friction is generated on these components when they translate which is essential for the propulsion of the device. At a time, a certain number of sliders move either forward or backward. The sliders that are moving forward are termed as advancing sliders and the sliders that are moving backward are termed as retracting sliders. The net friction force generated on the retracting sliders facilitates the forward motion of the device whereas the net friction force on the advancing sliders hinders the forward motion. For successful forward propulsion,

$$F_{retracting} > F_{advancing} \tag{1}$$

where, $F_{retracting}$ is the friction on retracting sliders and $F_{advancing}$ is the friction on advancing sliders. Thus, by moving more retracting sliders than the advancing slider, $F\_retracting$ becomes higher than $F\_advancing$. It is because the total area of contact between the sliders and the colon wall is higher for retracting sliders compared to advancing sliders. According to Coulomb's law of friction, the friction force is independent of the area of contact. However, this is only true when the surface of the two objects touching each other is rigid as they would only have three contact points irrespective of the surface area. When at least one of the surfaces becomes deformable the contact points almost tend to infinity and thus the friction becomes dependent on the surface area. In this case, the colon wall is a deformable surface, therefore the surface area influences the friction force.

The number of sliders is maximised in the design to increase the propulsion efficiency of the device inside the colon wall. The colon wall stretches when the sliders translate in the opposite direction because the colon wall moves along with the sliders due to its lower axial stiffness. Increasing the number of sliders decreases the amount of stretch in the colon wall due to the reduced width of the slider, thereby improving propulsion efficiency. Further, the increase in the number of sliders increases the difference between the friction on the retracting slider and friction on the advancing slider provided the number of advancing sliders at a time does not change, resulting in increased propulsion efficiency. The increase in the difference is due to the increased area of contact of the retracting sliders as well as the decreased area of contact of the advancing slider. The stroke length of the slider also influences the propulsion of the device. Stroke length of the slider is defined as the maximum length a slider can translate forward or backward. The distance that the colon wall can stretch before the slider could overcome the friction does not contribute to the propulsion distance. Thus, the stroke length has to be sufficiently high enough to enable the forward motion of the device. However, the stroke length influences the overall length of the device where the larger stroke length of the device affects the device's compactness.

B. Actuation system design

The device requires an actuation system to translate the sliders back and forth. There were three ideas of actuation proposed which includes the actuation of each slider using linear micromotors, the actuation of the sliders through a motor with a cam and the actuation of the sliders through a motor with a cam and springs. The representation of the ideas can be visualised in figure 7. The idea of using springs along with the motor and the cam was chosen as the better idea compared to the other two as it maximises the number of sliders. The actuation using linear micromotor resembles the actuation system present in the ovipositor of wasps where each slider requires induvial micromotors to translate. However, incorporating each micromotor would influence the number of sliders that can be present in the device due to space constraints. The actuation using a motor and a cam involves the motor as a single power source to deliver the force and the cam regulates the force accordingly to translate sliders. The cam has a surface profile consisting of two slopes namely forward and backward slopes. The backward slope provides the force to move the retracting slider and the forward slope provides the force to move the advancing slider. The slopes of the cam depends on the stroke length of the slider, the width of the slider and the number of sliders that can be present in their respective slopes for the given circumference of the cam. This can be represented by the following equations,

$$Tan\alpha = SL_s \div (W_s \times N_b) \tag{2}$$

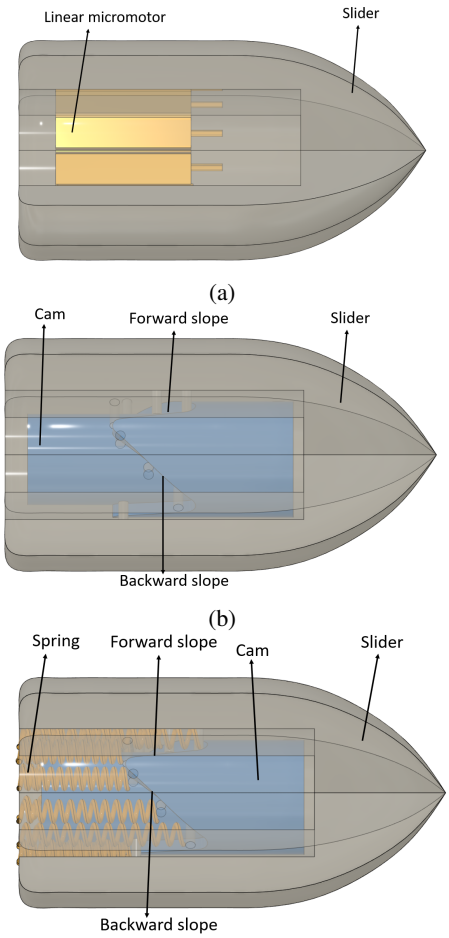

Fig. 7: Actuation system for sliders a. using linear micromotors, b.using a motor and a cam, c. using a motor, a cam and springs

$$Tan\theta = SL_s \div (W_s \times N_f) \tag{3}$$

$$2 \times \pi \times R_1 = W_s \times N_t) \tag{4}$$

$$N_t = N_b + N_f \tag{5}$$

Where, SL_s is the stroke length of the slider, W_s is the Width of the slider, θ is the angle of the forward slope, α is angle of the backward slope, N_b is the number of retracting sliders, N_f is the number of advancing slider, N_t is the total number of sliders in the device and R_1 is the minimum distance between the centre of the device to the distal part of the slider (distal indicates they are far away from the centre of the device and proximal indicates they are near to the centre of the device). Referring to the above equations, the number of sliders can be maximised by maximising the number of retracting sliders and the width of the slider provided the circumference remains constant. Maximising the number of advancing sliders to maximise the total number of sliders could be ignored as maximising advancing sliders would reduce the propulsion efficiency. Minimising the width of the sliders can be achieved by maximising the forward slope of the cam however, it would require very high torque from the motor to translate the advancing sliders where the torque required would tend to infinity as the forward slope tends to 90°. This issue can be resolved by using the springs to move the advancing sliders. The idea incorporates the use of compression springs for each individual slider. When the motor provides the torque to the cam, the backward slope of the cam translates the retracting sliders as well as compresses the spring. The energy stored in the spring is then used to move the advancing slider during the forward slope of the cam. This mechanism can be termed as spring loaded mechanism. Since the mechanism does not require any torque from the motor to translate the advancing slider, the forward slope of the cam can be as high as 90° thereby maximising the number of sliders present in the device.

C. Friction surface design

Friction between the retracting sliders and the colon wall plays a crucial role in propelling the device forward. The incorporation of gear-tooth like surface profiles in the sliders enhances the propulsion efficiency. The profiles increase the grip/friction acting between the slider and the colon wall due to the interlocking of the colon wall between the tooth. The colon wall is subjected to intra-abdominal pressure which interlocks the colon wall between the tooth. Since friction in the retracting sliders is necessary for propulsion, the interlocking helps in improving the propulsion efficiency of the device. A visual representation of the colon interlocking onto the surface profile of the sliders can be observed in figure 8.

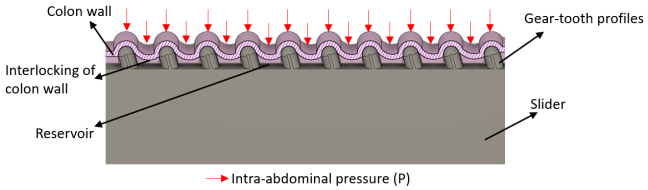

Fig. 8: Interlocking of colon wall

The colon wall consists of mucus of a certain thickness which hinders contact between the sliders and the colon wall. The gear-tooth like profiles helps in penetrating through the mucus layer thereby ensuring a good contact and further, the space between the profiles acts as the reservoir for the displaced mucus during tooth penetration. The displacement of mucus by the gear-tooth profiles is also necessary to achieve good contact with the colon wall. Frictional anisotropy was introduced by inclining the gear-tooth by an angle to the back of the device. This increases the friction on the retracting slider which supports the propulsion as well as reduces the friction on advancing sliders which hinders the propulsion.

IV. Detailed Design

The device designed consists of a total of 78 components which includes a main frame, a back cap, a motor, a cam, 4 set screws and 12 of each sliders, springs, rods and bearings.

Fig. 9: Assembled view

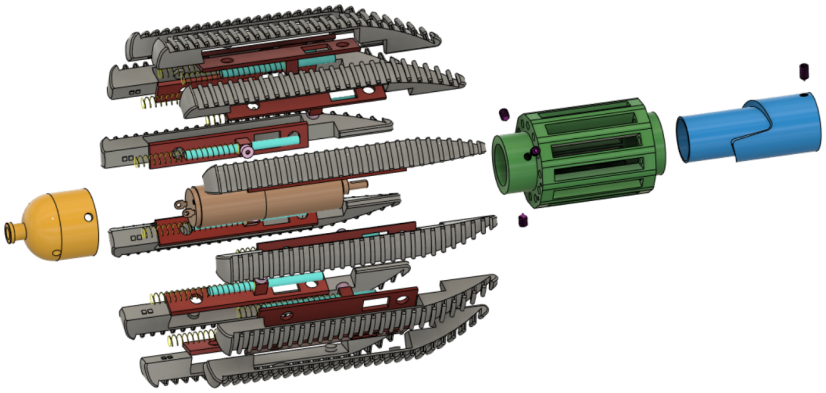

Fig. 10: Exploded view

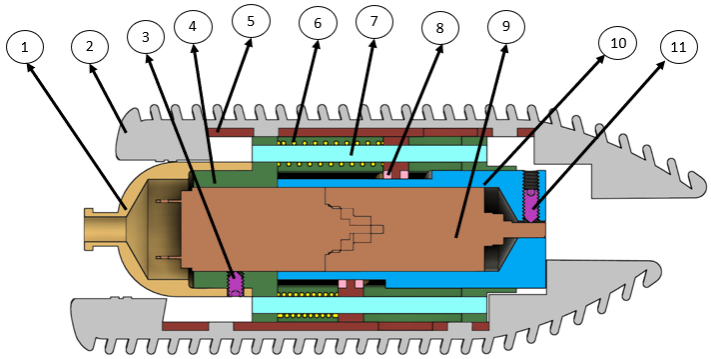

Fig. 11: Sectional view. 1.Back cap, 2. 3d printed attachment, 3. Set-screw to connect motor to the frame, 4. Main frame, 5. Slider, 6. Spring, 7. Rod, 8. Bearing, 9. Motor, 10.Cam, 11.Set-screw to connect cam to the shaft of the motor.

The maximum diameter of the device was around 29 mm with an approximate length of around 80 mm. The assembled view, exploded view and sectional view of the device design can be visualised in figure 9, 10 and 11. As discussed in the concept design, sliders are the components that can translate back and forth and are in direct contact with the colon wall. The retracting sliders are actuated by the motor and the cam whereas the advancing sliders are actuated by the spring. Bearings are used in the sliders to reduce the friction between the slider and the cam by converting the sliding contact into a rolling contact. The rod serves as the guide for the sliders to perform linear motion and restricts multiple degrees of freedom in the spring along with preventing the spring from buckling during compression.

A. Slider unit design

As discussed in the concept design, the number of sliders in the design has to be maximised. The calculation of the number of sliders depends on other components as each slider requires a rod, a bearing and a spring. However, the limiting factor for determining the number of sliders was the number of bearings because of less space availability when compared to other associated components. With this, the calculation was carried out which resulted in a maximum of 12 sliders. The calculation for determining the number of sliders is given in the appendix A. The sliders have a stroke length of 1 cm to ensure effective propulsion of the device without affecting the compactness of the device. The sliders were made out of two parts, a metal part and a 3d printed part where the 3d

printed part would be in contact with the colon wall whereas the metal part is placed below the 3d printed part. There were two notable advantages of designing the sliders as two separate parts. Firstly, the 3d printed part offers enhanced friction with the colon wall compared to the metal part which is necessary for the propulsion. Secondly, the surface profile of the 3d printed part could be easily modified and manufactured, which is not easily achievable with metal manufacturing.

The outer surface of the 3d printed part was given an inverse parabolic shape to open up the closed colon without inflicting any damage to the colon. If the device is entirely covered by the colon, the slider requires no additional force to open up the colon, in spite of the intra-abdominal pressure, as the force required to open the colon is counterbalanced by the force of closing the colon, resulting in zero net force. A corresponding illustration of this phenomenon can be found in figure 12. The surface of the 3d printed part consists of gear tooth like profiles that are inclined to the back of the device at an angle of 15°. This inclination introduces frictional anisotropy wherein the retracting sliders experience greater friction than the advancing slider, thereby increasing the propulsion efficiency. The minimum height of the tooth was chosen as 1.5 mm to ensure the tooth penetrates successfully through the mucus and establishes good contact with the colon wall. Since the displacement of mucus by the tooth is necessary to achieve good contact with the colon wall, the volume of the space between the tooth was designed to be higher than the volume of the tooth to ensure there is sufficient space for the mucus to get displaced. The tooth was concavely curved to achieve a circular section when the device is fully assembled.

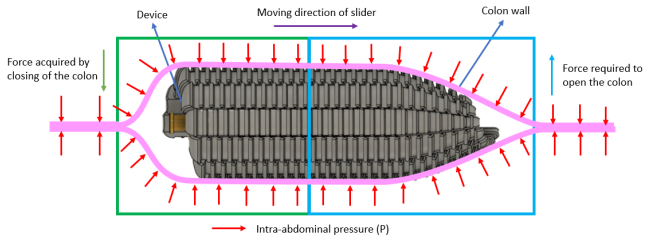

Fig. 12: Subjection of intra-abdominal pressure on the device inside a colon

The metal part of the slider consists of two holes at the top for securely attaching the 3d printed part. The bearings are attached to the metal slider to minimize friction between the slider and the cam, facilitating smooth movement. The rods are inserted into the metal part which acts as a linear guide to the slider and also restricts multiple degrees of freedom in the spring along with preventing the spring from buckling during compression.

The springs are used to provide force to the advancing slider and reduce the torque required by the motor to translate retracting sliders and compress the springs. The calculation of the force required by the spring depends on internal friction in the device and friction force between the slider and the colon which makes the calculation complex. Thus, the springs were selected based on trial and error method. Springs with different specifications were chosen and the best spring is selected based on their ability to push the advancing slider. Additionally, an initial compression of 5 mm was applied to the springs within the device to maintain a minimum force on the slider. This prevents the advancing slider from stopping before it reaches the stroke length due to friction between the advancing slider and the colon wall. Moreover, the minimum force from the spring ensures the motor receives support continuously, alleviating the need for it to generate the entire force independently. An assembled view of a single slider, rod, spring, and bearing can be observed in figure 13.

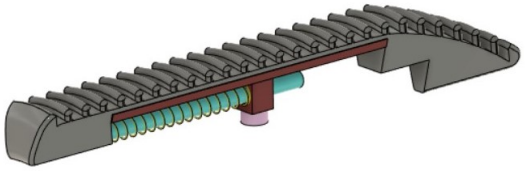

Fig. 13: Assembly of slider and its associated components

B. Cam design

The introduction of springs offers the possibility of achieving a forward slope as high as 90°, thereby maximizing the number of sliders in the design. However, the forward slope in the cam design was chosen slightly less than 90° to reduce the torque required by the motor. The spring moving the advancing slider also provides the torque to the cam to move the retracting slider and compress the spring thereby supporting the motor. In contrast, when the forward slope is at 90°, the energy stored in the spring is solely dedicated to the advancing slider without any additional support to the motor. The equation 6 and 7 represent the force required by the motor when there is no support from the spring and when there is support from the spring respectively. Also, equation 8 represents the torque required by the motor.

$$F_m = F_{sb1}tan\alpha + F_{sb2}tan\alpha + F_{sb3}tan\alpha + ...F_{sbn}tan\alpha \quad (6)$$

$$\begin{aligned} F_m =& (F_{sb1}tan\alpha + F_{sb2}tan\alpha + F_{sb3}tan\alpha + ...F_{sbn}tan\alpha) - \\ & (F_{sf1}tan\theta + F_{sf2}tan\theta + F_{sf3}tan\theta + ...F_{sfn}tan\theta) \end{aligned} \quad (7)$$

$$T_m = F_m * R_2 \quad (8)$$

Where, F_m is the force required by the motor, F_{sb1}, F_{sb2}, ..., F_{sbn} is the force on the spring 1 to spring n that are present on the backward slope of the cam, F_{sf1}, F_{sf2}, ..., F_{sfn} is the force on the spring 1 to spring n that are present on the forward slope of the cam. The force equation derivation is given in appendix B. The profile of the cam was created such that there is only one slider on the forward slope of the cam and this profile exists on only one side of the cam. The advantage of having a one-sided cam profile is that the mechanism does not get affected even if the spring is unable to completely push the advancing slider to its full stroke length.

There were in total of three different cams designed namely 1-jump camp, 2-jump cam and 3-jump cam. The 1-jump cam, 2-jump cam and 3-jump cam consist of one forward/backward slope, two forward/backward slopes and three forward/backward slopes respectively. The figure 14 illustrates the 2d representation of cam profiles for the three

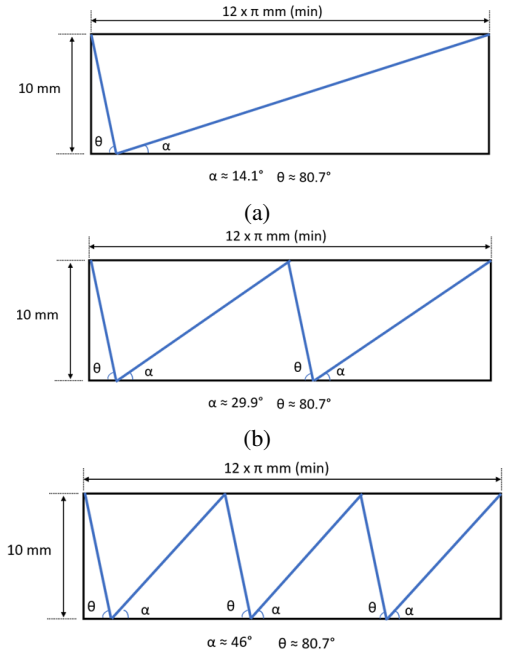

Fig. 14: a. 2D profile of 1-jump cam. b. 2D profile of 2-jump cam. c. 2D profile of 3-jump cam

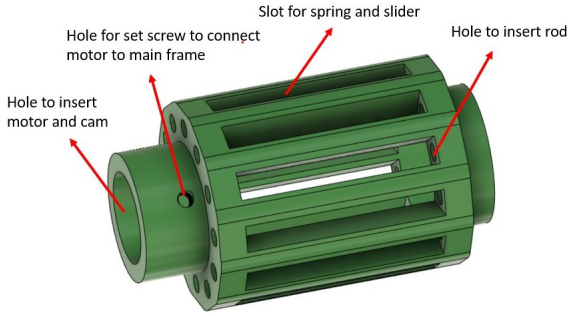

Fig. 15: Main frame

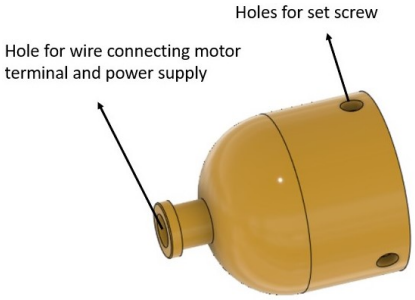

Fig. 16: Back cap

different cams. The primary objective behind these different cam designs was to assess their impact on propulsion efficiency and speed of the device as theoretically, the 3-jump cam would propel faster than the 2-jump cam followed by the 1-jump cam. However, the friction ratio of retracting to advancing slider would be less for 3-jump cam compared to 2-jump and 1-jump cam due to the reduced number of retracting sliders and increased number of advancing sliders at a time, thereby affecting the propulsion efficiency of the device.

C. Motor & frame design

The motor was selected based on the torque required to translate retracting sliders as well as to charge the springs. The torque calculation was specifically focused on the 3-jump cam, as it necessitates more torque due to its higher backward slope compared to the 1-jump and 2-jump cams. There were two assumptions made during the calculation. First, The force required to compress the springs is fully delivered by the motor (i.e. the spring in the forward slope does not help to reduce the force required by the motor to compress the springs). Second, The force acting on the spring is constant and equal to the average between the force in the spring when they are compressed till the end of the slider's stroke (15 mm) and the force in the spring due to their initial compression (5 mm). The calculation resulted in a torque value of around 39 N mm, however, various other factors could influence the torque required by the motor such as internal friction of the device which is very difficult to evaluate. Thus, considering a safety factor, the motor of torque value 100 N mm was selected. The torque calculation is elaborated in appendix C. The shaft of the motor is attached to the cam with the help of a set screw to ensure proper rotation of the cam by the motor.

The frame consists of two parts namely, the main frame and the back cap. The frame was made as two separate parts due to ease of manufacturing and assembly. The main frame features a polygon shape with 12 sides to accommodate one slider on each side. Further, each side has a rectangular slot to accommodate the springs and provides space for the sliders to translate back and forth. Additionally, the main frame consists of 12 holes that are concentric to the spring diameter and holds the rod in its place with the help of friction. Finally, the main frame has a hole at the centre to insert the motor as well as the cam and is held together with the help of set screws. The back cap consists of a hollow cylinder with a dome to cover the back of the motor and the wire connection. There is a small hole at the back to pass through the wire that connects the motor terminal with the power supply. The main frame and the back cap protect the motor as well as the wire connected at the motor terminal from exposure to the colon wall. The illustration of the main frame and the back cap can be visualised in figure 15 and 16.

D. Prototype development

The prototype of the design was developed involving the production of components such as the main frame, back cap, cams and sliders at DEMO in Delft University of Technology. These components were manufactured using Aluminium (7075 – T5) due to their low density contributing to reduced overall component weight. The 3d printed part of the slider was manufactured in the BITE lab at the Delft University of Technology using Stereolithography (SLA) printing. Finally, the springs, rods and bearings were purchased as standard products. The exploded view, partially assembled view and

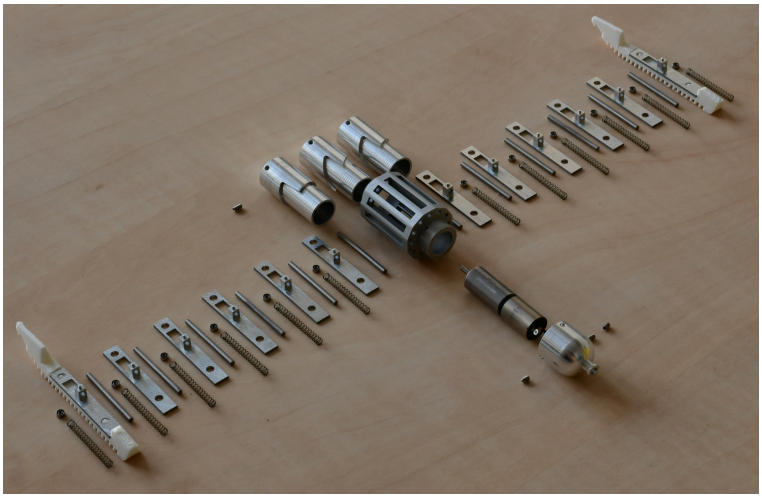

Fig. 17: Exploded view of the prototype

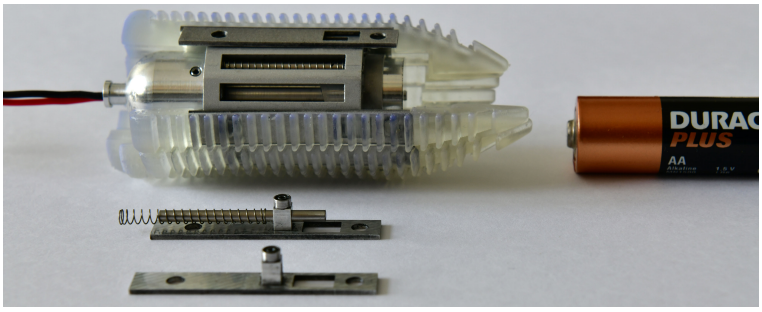

Fig. 18: Partially exploded view of the prototype

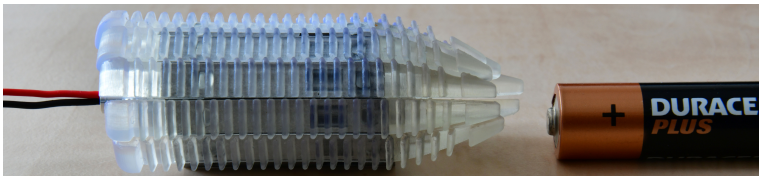

Fig. 19: Assembled view of the prototype

fully assembled view of the prototype can be observed in figure 17, 18 and 19.

V. Experiment

A. Construction of experiment set-up

The experimental investigation involved testing the propulsion of the prototype in a simulated colon environment. The simulated colon environment was built manually and there were three features mimicked which include stiffness of the colon wall, slipperiness of the colon wall and intra-abdominal pressure acting on the colon wall. Friction between the sliders of the device and the colon wall is an important component that is necessary for the device's propulsion. The colon wall's lower stiffness, coupled with the intra-abdominal pressure would wrap the colon around the device, exerting a circumferential pressure on the device thereby affecting the friction between the sliders of the device and the colon wall. Further, the slipperiness due to the mucus present in the colon wall also influences friction. Thus, these three features were mimicked in the colon-simulated environment. A colon phantom was prepared from a plastic bag [38]. The plastic bag was cut into a rectangular sheet and folded into a pipe-like structure. There were multiple colon phantoms prepared where each of the folded regions of the phantom was joined together either by glue, cello tape or rubber seal tape [39]–[41]. The colon phantom had an approximate diameter of 37 mm and an approximate length of 400 mm. The diameter of the colon phantom was kept constant throughout the entire phantom owing to the simplification of the model in contrast to the real colon where the diameter varies at different sections. Further, the diameter of the colon phantom was kept higher than the maximum diameter of the device to prevent any radial stretching of the colon phantom. To mimic the presence of mucus in the colon, sunflower oil [42] was utilized. A small amount of oil was manually spread within the colon phantom to replicate the slipperiness caused by the mucus present in the actual colon. In a real colon, there are typically two mucus

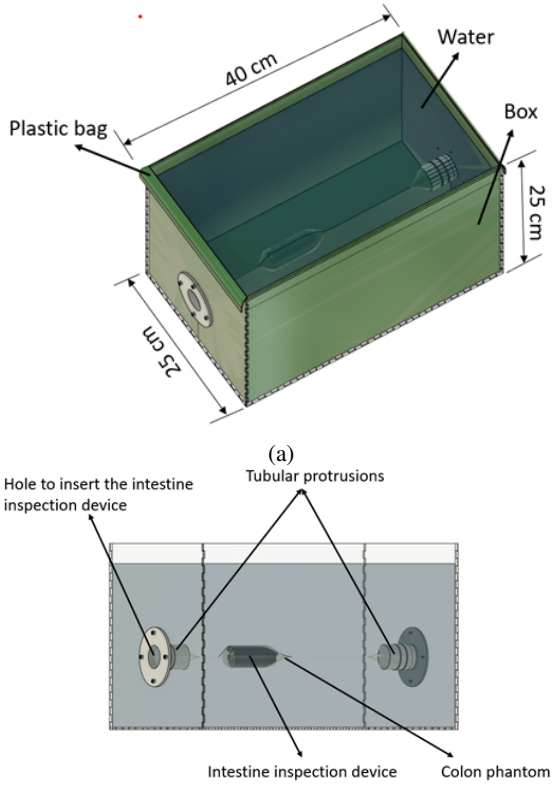

Fig. 20: Schematic representation of experiment set-up, a. with plastic cover, b. without plastic cover

layers - the inner layer and the outer layer. The inner layer is attached to the colon wall whereas the outer layer remains unattached and less dense [43]. There is no constant value for mucus thickness in the colon as they are dynamic and vary with time [44]. However, due to the complexity, the dynamic nature of the mucus thickness was not implemented in the colon phantom.

The intra-abdominal pressure was emulated using water pressure. The intra-abdominal pressure in the human colon ranges from 0.67 kPa to 0.93 kPa [45] and the average value of the intra-abdominal pressure was taken as the base value (0.8 kPa). To replicate this pressure condition, a colon phantom was submerged in water to a depth of 8 cm. A box was fabricated from PMMA of dimensions 40 cm x 25 cm x 25 cm (l x b x h) to hold the water. Each side of the box was laser cut and joined together with the help of silicon caulk and rubber seal tape. The box consist of two holes on either side along the length on to which tubular protrusions were attached using screws. The tubular protrusions were created from PLA and serves as the mount for the colon phantom. The colon phantom as well as the box is covered with a plastic bag [46] and then water is filled to prevent the water from entering the colon phantom as it would inflict damage to the prototype. Further, the plastic bag prevents the water from leaking outside the box. The schematic representation of the experiment setup with and without the plastic bag can be visualised in figure 20. The experiment set-up with the device inside the colon phantom can be visualised in the figure 21.

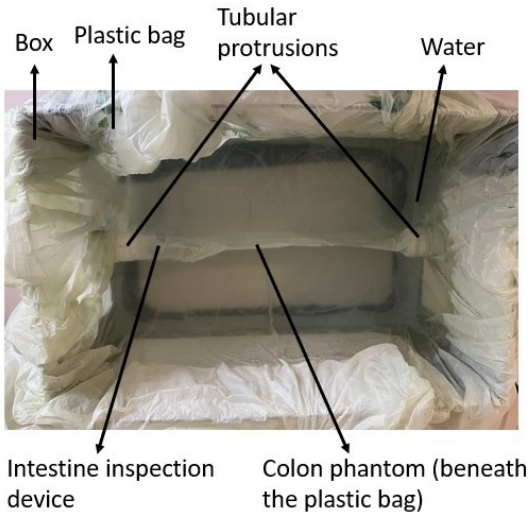

Fig. 21: Experiment set-up

B. Experimental procedure

Initially, the colon phantom was secured to the tubular protrusions with the help of rubber bands. The plastic bag was used to cover the colon phantom and the box. A thread was attached to the back of the device, enabling its return to the starting position after each trial. Before filling the box with water, the intestine inspection device was inserted through one of the tubular protrusions until the entire device has contact with/surrounded by the colon phantom. Later, the water was filled such that the colon phantom is submerged in the water at a depth of 8 cm. There were in total of nine trials conducted and all the trials were carried out at the maximum speed of the motor possible (12 V) along with the 1-jump cam. The device was allowed to autonomously propagate along a distance of approximately 240 mm. The trials of the experiment were video recorded. The trials were done in quick succession where as soon as the device reaches the end, it was pulled back and the next trial was initiated unless intervention was necessary during the experiment.

C. Results

The inspection device for the intestine demonstrated successful propagation through the colon phantom in six out of nine trials, covering an approximate distance of 240 mm in an average of around 43s. The average velocity of the device propulsion inside the colon phantom was 5.68 mm/s. The results of the successful trials can be visualised in table II. The cluster indicates the trials experimented in quick succession. The propulsion efficiency of the device was calculated as follows,

$$Theoretical\ distance(T_d) = SL \times N_s$$

$$Propulsion\ efficiency = (T_d \div E_d) \times 100$$

Where SL is the stroke length of the slider, N_s is the number of rotations taken by the device to propagate till the experiment

TABLE II: Results

Trial no.	Experimental distance (mm)	Stroke length (mm)	Number of rotation	Theoretical distance (mm)	Efficiency (%)	Time taken by the device to cover the experiment distance (s)	Velocity (mm/s)	Colon phantom joining method	Cluster no
1	240	10	28	280	85.71	36	6.67	cello tape	1
1	240	10	34	340	70.59	44	6.67	cello tape	1
1	240	10	29	290	82.76	39	6.15	cello tape	1
1	240	10	33	330	72.72	42	5.71	cello tape	1
1	240	10	40	400	60	49	4.90	rubber seal tape	2
1	240	10	38	380	63.16	46	5.22	rubber seal tape	2

distance and E_d is the experiment distance. The device had an average efficiency of around 72.5 % where the efficiency of the device was higher during cluster 1 compared to cluster 2. There were in total 3 unsuccessful trials due to very less/no propagation of the device after setting up the experiment and also due to the tearing of the colon phantom joined by cello tape during one of the trials. The device required a manual run through the colon phantom after setting up the experiment as the device was not able to propagate or propagated very slowly prior to the manual run. The manual run was carried out by pushing the device manually from one end of the colon phantom to the other. The colon phantom, created by joining rectangular sheets using rubber seal tape, exhibited better durability compared to the phantom joined with glue or cellop tape, as the latter shredded at the joint location when exposed to oil. The durability of the phantom joined by glue was the least as they shredded rapidly after the oil exposure. After the trials, the visual observation of the device indicated a minute amount of oil/water infusion within the device which can be seen in figure 22.

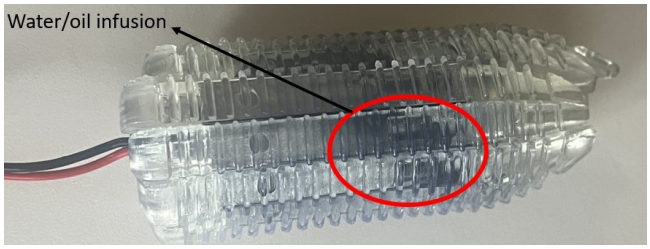

Fig. 22: Oil/water infusion inside the device

VI. Discussion & Future research

The reduction in the propulsion efficiency could be associated with various factors which includes slip in the retracting sliders due to oil and lack of spring force to translate the advancing slider to its stroke length. Further, there is significant difference in the propulsion efficiency between clusters which could be associated with the use of the colon phantom prepared by a different joining method and the difference in setting up the experiment. Since the colon phantom is submerged in the water and a plastic bag was used to protect the colon phantom, it was very difficult during the set-up phase of the experiment to keep the colon phantom in a straight line and it also proved difficult to observe the device during propulsion which hindered the identification of the exact reason for reduced efficiency.

The reason for the very slow/no propagation of the device before the manual run could be attributed to the capillary adhesion inside the colon phantom. Since the colon phantom remains closed due to water pressure, the walls of the colon phantom come into contact with each other, with a layer of oil in between. The walls of the colon phantom adhere via the surface tension, resulting in capillary adhesion [47]. It requires an additional force by the device to overcome this adhesion causing very slow/no propagation inside the colon phantom. However, the effect of capillary adhesion depends on time and a research study proved that it requires a sufficient amount of time for the surfaces to adhere [47]. Since setting up the experiment required a considerable amount of time, the capillary adhesion would come into action. Upon the manual run, the capillary adhesion would have been eliminated as the next sets of trials were made in quick succession. The other possible reason for very slow/ no propagation before the manual run is the uneven spread of the oil as the oil was spread throughout the colon phantom manually. During the manual run of the device, the sliders of the device could have facilitated an even oil spread throughout the colon phantom resulting in easier propagation of the device in successive trials. Though the capillary adhesion and uneven oil spread inside the colon phantom could be attributed to the inability of the device to propagate successfully before the manual run, these reasons are speculative and require further investigation which is outside the scope of the study. There is a drawback to the current preparation method of the colon phantom as at the joint location, the phantom would not exhibit the stretching property of the colon due to the adhesion of the cello tape or rubber seal tape. To partially mitigate this drawback, a plastic film sealer could be employed instead of a tape, as it would minimize the area of the joint section, resulting in less area where the stretching ceases to exist.

The intestine inspection device was able to propagate in the colon-simulated environment. However, it is necessary to conduct experiments in an actual colon to validate the device's effectiveness. On successful propagation of the device inside the real colon, different values such as speed of propagation, slip, etc. could be quantified. Additionally, the experiments can be performed with different cams to verify the speed of the propagation or slip as theoretically, the 3-jump cam should be able to move faster than the 2-jump cam followed by the 1-jump cam. Finally, different surface profiles of the 3d printed

part of the slider such as pillar profile and central space wall profile could be tested. These profiles offer increased space for mucus flow compared to the wall profile, which is crucial for ensuring good contact between the device and the colon wall to generate friction. Thus, experimenting with different surface profiles could determine their influence on the propagation of the device. The pillar profile and central space wall profile can be visualised in figure 23. The current device consists of many components due to maximising the number of sliders which in turn increases the assembly and disassembly time. The number of sliders was maximised to reduce the stretching of the colon wall which hinders the device's propulsion. The stretching of the colon wall occurs at the interface where the sliders translate in the opposite direction and can be prevented by reducing the friction between the advancing slider and the colon wall to zero. Thus, incorporating friction anisotropy in the future design of the sliders where it exhibits zero friction while translating forward and maximum friction while translating backward would drastically reduce the number of components in the device. Finally, the device requires a redesign in terms of length reduction or flexibility as research suggests that the maximum length of the rigid parts in a self-propelled colonoscopic device should be a maximum of 4 cm [48].

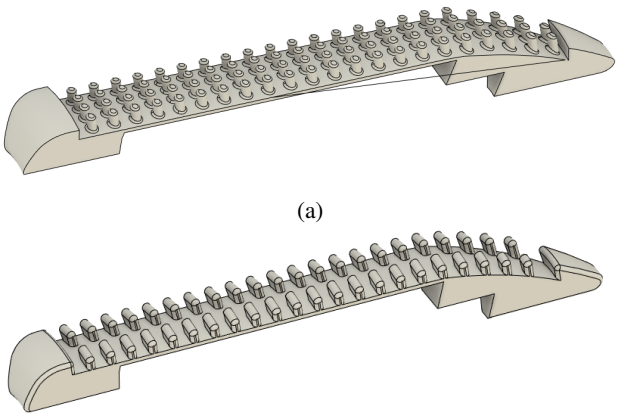

(a)

(b)

Fig. 23: a. Pillar profile, b. Central space wall profile

VII. Conclusion

In this study, a proof of concept for a self-propelled colonoscopic device inspired by the ovipositor of wasps was conducted. Various studies were carried out in developing devices inspired from the locomotion of earthworms however its propulsion was hindered due to friction and low axial stiffness of the colon wall. Inspiration was taken from the ovipositor of wasps as they can penetrate into the tree bark despite its slenderness. A prototype was developed and tested in a colon-simulated environment. The device was able to successfully propagate through the colon phantom but the device required an initial manual run through the phantom after setting up the experiment. There were two major reasons attributed to the required initial manual run - to eliminate the capillary adhesion inside the colon phantom due to the oil and to spread the oil evenly throughout the colon phantom. However, these reasons were speculative and further investigation was required which was outside the scope of the study. The device had an average velocity of around 5.68 mm /s inside the colon phantom with an average efficiency of 72.5%. As a future study, the device has to be experimented inside a real colon to test the working of the device and its propulsion efficiency. Additionally, the device design could be improved by minimising the number of components. This could be achieved by enabling the sliders to exhibit zero friction during forward translation and maximum friction during backward translation.

Acknowledgement

I would like to thank my supervisors Paul Breedveld and Mostafa Atalla for supporting me throughout the graduation project. Further, I would like to express my gratitude to Remi van Starkenburg from DEMO for providing support related to the design of the prototype and manufacturing of the prototype. Finally, I would like to thank David Jager from DEMO for manufacturing of the prototype.

References

[1] D. K. Rex, P. S. Schoenfeld, J. Cohen, I. M. Pike, D. G. Adler, M. B. Fennerty, J. G. Lieb, W. G. Park, M. K. Rizk, M. S. Sawhney, and et al., "Quality indicators for colonoscopy," *Gastrointestinal Endoscopy*, vol. 81, no. 1, p. 31–53, 2015.

[2] S.-A. Abad, A. Arezzo, S. Homer-Vanniasinkam, and H. A. Wurdemann, "Soft robotic systems for endoscopic interventions," *Endorobotics*, p. 61–93, 2022.

[3] C. Klabunde, D. Joseph, J. King, A. White, and M. Plescia, "Vital signs: Colorectal cancer screening test use - united states, 2012," *Morbidity and Mortality Weekly Report*, vol. 62, pp. 881–888, 11 2013.

[4] "Colorectal cancer statistics," Jun 2022. [Online]. Available: https://www.cdc.gov/cancer/colorectal/statistics/index.htm

[5] "What is colorectal cancer," Mar 2023. [Online]. Available: https://digestivecancers.eu/colorectal-what/

[6] "Colorectal cancer burden in eu-27," Mar 2021. [Online]. Available: https://ecis.jrc.ec.europa.eu/pdf/Colorectal_cancer_factsheet-Mar_2021.pdf

[7] H. Sharif, C. L. Hoad, N. Abrehart, P. A. Gowland, R. C. Spiller, S. Kirkham, S. Loganathan, M. Papadopoulos, M. A. Benninga, D. Devadason, and et al., "Colonic volume changes in paediatric constipation compared to normal values measured using mri," *Diagnostics*, vol. 11, no. 6, p. 974, 2021.

[8] C. M. Stauffer, "Colonoscopy," Feb 2023. [Online]. Available: https://www.statpearls.com/ArticleLibrary/viewarticle/19735

[9] "The colon: What it is, what it does and why it is important." [Online]. Available: https://fascrs.org/patients/diseases-and-conditions/a-z/the-colon-what-it-is,-what-it-does

[10] T. D. Schmidt, "Colonoscopy," *Encyclopedia of Gastroenterology*, p. 449–456, 2004.

[11] C. Whelan, "What to eat after a colonoscopy," Jun 2019. [Online]. Available: https://www.healthline.com/health/what-to-eat-after-colonoscopy

[12] A. J. Loeve, P. Fockens, and P. Breedveld, "Mechanical analysis of insertion problems and pain during colonoscopy: Why highly skill-dependent colonoscopy routines are necessary in the first place... and how they may be avoided," *Canadian Journal of Gastroenterology*, vol. 27, no. 5, p. 293–302, 2013.

[13] H. Dehghani, C. R. Welch, A. Pourghodrat, C. A. Nelson, D. Oleynikov, P. Dasgupta, and B. S. Terry, "Design and preliminary evaluation of a self-steering, pneumatically driven colonoscopy robot," *Journal of Medical Engineering & Technology*, vol. 41, no. 3, p. 223–236, 2017.

[14] A. Loeve, D. Plettenburg, P. Breedveld, and J. Dankelman, "Endoscope shaft-rigidity control mechanism: "forguide"." *IEEE Trans. Biomed. Engineering*, vol. 59, pp. 542–551, 01 2012.

[15] S. Park, H. Park, S. Park, and B. Kim, "A paddling based locomotive mechanism for capsule endoscopes," *Journal of Mechanical Science and Technology*, vol. 20, no. 7, p. 1012–1018, 2006.

[16] T. Rösch, A. Adler, H. Pohl, E. Wettschureck, M. Koch, B. Wiedenmann, and N. Hoepffner, "A motor-driven single-use colonoscope controlled with a hand-held device: A feasibility study in volunteers," *Gastrointestinal Endoscopy*, vol. 67, no. 7, p. 1139–1146, 2008.

[17] C. Mosse, T. N. Mills, M. N. Appleyard, S. S. Kadirkamanathan, and C. Swain, "Electrical stimulation for propelling endoscopes," *Gastrointestinal Endoscopy*, vol. 54, no. 1, pp. 79–83, 2001. [Online]. Available: https://www.sciencedirect.com/science/article/pii/S0016510701385899

[18] C. Sevcencu, N. J. M. Rijkhoff, H. Gregersen, and T. Sinkjaer, "Propulsive activity induced by sequential electrical stimulation in the descending colon of the pig," *Neurogastroenterology & Motility*, vol. 17, no. 3, pp. 376–387, 2005. [Online]. Available: https://onlinelibrary.wiley.com/doi/abs/10.1111/j.1365-2982.2004.00637.x

[19] M. Shike, Z. Fireman, R. Eliakim, O. Segol, A. Sloyer, L. B. Cohen, S. Goldfarb-Albak, and A. Repici, "Sightline colonosight system for a disposable, power-assisted, non-fiber-optic colonoscopy (with video)," *Gastrointestinal Endoscopy*, vol. 68, no. 4, pp. 701–710, 2008. [Online]. Available: https://www.sciencedirect.com/science/article/pii/S001651070800014X

[20] J. Pfeffer, R. Grinshpon, D. Rex, B. Levin, T. Rösch, N. Arber, and Z. Halpern, "The aer-o-scope: Proof of the concept of a pneumatic, skill-independent, self-propelling, self-navigating colonoscope in a pig model," *Endoscopy*, vol. 38, no. 2, p. 144–148, 2006.

[21] S. A. Coleman, M. Pakleppa, and A. Cuschieri, "Hydro-jet propelled colonoscopy: Proof of concept in a phantom colon," *Surgical Endoscopy*, vol. 35, no. 2, p. 989–995, 2020.

[22] L. Manfredi, "Endorobots for colonoscopy: Design challenges and available technologies," *Frontiers in Robotics and AI*, vol. 8, 2021.

[23] W. Li, W. Guo, M. Li, and Y. Zhu, "A novel locomotion principle for endoscopic robot," in *2006 International Conference on Mechatronics and Automation*, 2006, pp. 1658–1662.

[24] S. White, "A flexible body allows the earthworm to burrow through soil - biological strategy - asknature," Jul 2020. [Online]. Available: https://asknature.org/strategy/a-flexible-body-allows-the-earthworm-to-burrow-through-soil/

[25] F. Cosentino, E. Tumino, G. R. Passoni, E. Morandi, and A. Capria, "Functional evaluation of the endotics system, a new disposable self-propelled robotic colonoscope: in vitro tests and clinical trial," *The International Journal of Artificial Organs*, vol. 32, no. 8, p. 517–527, 2009.

[26] P. Dario, M. Carrozza, L. Lencioni, B. Magnani, and S. D'Attanasio, "A microrobotic system for colonoscopy," in *Proceedings of International Conference on Robotics and Automation*, vol. 2, 1997, pp. 1567–1572 vol.2.

[27] J. Zuo, G. Yan, and Z. Gao, "A micro creeping robot for colonoscopy based on the earthworm," *Journal of Medical Engineering & Technology*, vol. 29, no. 1, p. 1–7, 2005.

[28] B. Kim, S. Lee, J. Park, and J.-O. Park, "Design and fabrication of a locomotive mechanism for capsule-type endoscopes using shape memory alloys (smas)," *IEEE/ASME Transactions on Mechatronics*, vol. 10, no. 1, p. 77–86, 2005.

[29] B. Kim, S. Park, C. Jee, and S.-J. Yoon, "An earthworm-like locomotive mechanism for capsule endoscopes," 09 2005, pp. 2997 – 3002.

[30] C. Stauffer and C. Pfeifer. In: StatPearls [Internet], 2023. [Online]. Available: https://www-ncbi-nlm-nih-gov.tudelft.idm.oclc.org/books/NBK559274/

[31] [Online]. Available: https://training.seer.cancer.gov/colorectal/anatomy/#:~:text=The\%s20entire\%20colon\%20is\%20about,by\%20peritoneal\%20folds\%20called\%20mesentery

[32] C. C. m. professional, "Colonoscopy: Prep amp; procedure details." [Online]. Available: https://my.clevelandclinic.org/health/diagnostics/4949-colonoscopy

[33] P. Breedveld, "Development of a rolling stent endoscope," in *The First IEEE/RAS-EMBS International Conference on Biomedical Robotics and Biomechatronics, 2006. BioRob 2006.*, 2006, pp. 921–926.

[34] M. Scali, T. P. Pusch, P. Breedveld, and D. Dodou, "Ovipositor-inspired steerable needle: Design and preliminary experimental evaluation," *Bioinspiration & Biomimetics*, vol. 13, no. 1, p. 016006, 2017.

[35] N. M. van Meer, U. Cerkvenik, C. M. Schlepütz, J. L. van Leeuwen, and S. W. Gussekloo, "The ovipositor actuation mechanism of a parasitic wasp and its functional implications," *Journal of Anatomy*, vol. 237, no. 4, p. 689–703, 2020.

[36] U. Cerkvenik, B. van de Straat, S. W. Gussekloo, and J. L. van Leeuwen, "Mechanisms of ovipositor insertion and steering of a parasitic wasp," *Proceedings of the National Academy of Sciences*, vol. 114, no. 37, 2017.

[37] L. Frasson, S. Y. Ko, A. Turner, T. Parittotokkaporn, J. F. Vincent, and F. Rodriguez y Baena, "Sting: A soft-tissue intervention and neurosurgical guide to access deep brain lesions through curved trajectories," *Proceedings of the Institution of Mechanical Engineers, Part H: Journal of Engineering in Medicine*, vol. 224, no. 6, p. 775–788, 2009.

[38] [Online]. Available: https://www.jumbo.com/producten/jumbo-pedaalemmerzakken-hoog-30-liter-20-stuks-163368ROL

[39] [Online]. Available: https://www.amazon.in/Pidilite-Industries-Fevistik-25g/dp/B07N85Y5L7

[40] [Online]. Available: https://www.hema.nl/vrije-tijd-kantoor/klussen/overige-klusartikelen/verpakkingstape-81040056.html

[41] [Online]. Available: https://www.praxis.nl/bouwmaterialen/bouwbenodigdheden/tape-lijm/technisch-tape/bison-reparatietape-rubber-seal-tape/10000821

[42] [Online]. Available: https://www.jumbo.com/producten/jumbo-zonnebloemolie-1l-331242FLS?channable=02a13d6964003333331323432464c53a9\&ju_subth=b2c

[43] M. E. Johansson, H. Sjövall, and G. C. Hansson, "The gastrointestinal mucus system in health and disease," *Nature Reviews Gastroenterology & Hepatology*, vol. 10, no. 6, p. 352–361, 2013.

[44] J. K. Gustafsson, A. Ermund, M. E. Johansson, A. Schütte, G. C. Hansson, and H. Sjövall, "An ex vivo method for studying mucus formation, properties, and thickness in human colonic biopsies and mouse small and large intestinal explants," *American Journal of Physiology-Gastrointestinal and Liver Physiology*, vol. 302, no. 4, 2012.

[45] D. Dodou, "Colonic locomotion," *Mechanical, Maritime and Materials Engineering, Delft University of Technology*, Sep 2006. [Online]. Available: http://resolver.tudelft.nl/uuid:0333b46c-8706-4aeb-b308-b69af9b99cf9

[46] [Online]. Available: https://www.ah.nl/producten/product/wi186602/ah-containerzakken-240-liter

[47] M. Butler, "Sticking with droplets: How having a soft foot can improve capillary adhesion," Aug 2019. [Online]. Available: https://ima.org.uk/12249/sticking-with-droplets-how-having-a-soft-foot-can-improve-capillary-adhesion/

[48] I. Kassim, L. Phee, W. Ng, F. Gong, P. Dario, and C. Mosse, "Locomotion techniques for robotic colonoscopy," *IEEE Engineering in Medicine and Biology Magazine*, vol. 25, no. 3, p. 49–56, 2006.

APPENDIX A
CALCULATION FOR DETERMINING MAXIMUM NUMBER OF SLIDERS

The minimum distance between the centre of the device and to proximal part of the bearing (R_b) = 11 mm

Available space (S_b) = $R_b \times \pi$ = 34.56 mm

Outer diameter of the bearing (OD_b) = 3 mm

Number of bearings that could be attached in the available space = $S_b \div OD_b$ = 11.52 $\equiv$ 12

The approximate area of intersection would be the area right angled triangle where the length of the triangle is the maximum intersection possible and height of the triangle is the difference in the radial distance between the centre of the device to the point of maximum intersection and the radial distance between the centre of the device to the point of zero intersection.

Number of bearing (N_b) = 12

Outer diameter of the bearing (OD_b) = 3 mm

The minimum distance between the centre of the device and to proximal part of the bearing (R_b) = 11 mm

Available space (S_b) = $R_b \times \pi$ = 34.56 mm

Length of triangle (l) = $((N_b \times OD_b) - S_b) \div 12$

= 0.12 mm

Radial distance between the centre of the device to the point of maximum intersection (R_{bmax}) = R_b

Radial distance between the centre of the device to the point of zero intersection (R_{bmin}) = $(N_b \times OD_b) \div \pi$ = 11.46 mm

Height of the triangle (h) = $R_{bmax} - R_{bmin}$ = 0.46 mm

The approximate area of intersection is then given by,

= ½ * h * l

= 0.0276 mm2

APPENDIX B
MOTOR FORCE DERIVATION

Consider 4 sliders with springs on a cam profile where one slider is on the forward slope of the profile and the 3 sliders are on the backward slope of the profile as could be seen in figure 24.

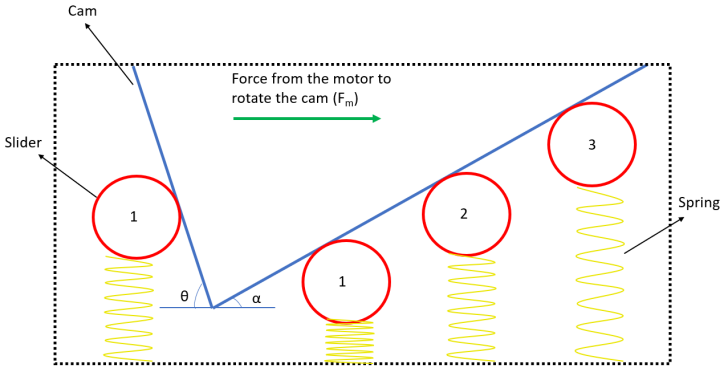

Fig. 24: Example of spring loaded mechanism

The net horizontal force acting on the cam profile due to springs is the necessary component contributing to the torque of the motor. The net horizontal force acting on the cam profile can be calculated from the free body diagram (FBD) which is given in the figure 25.

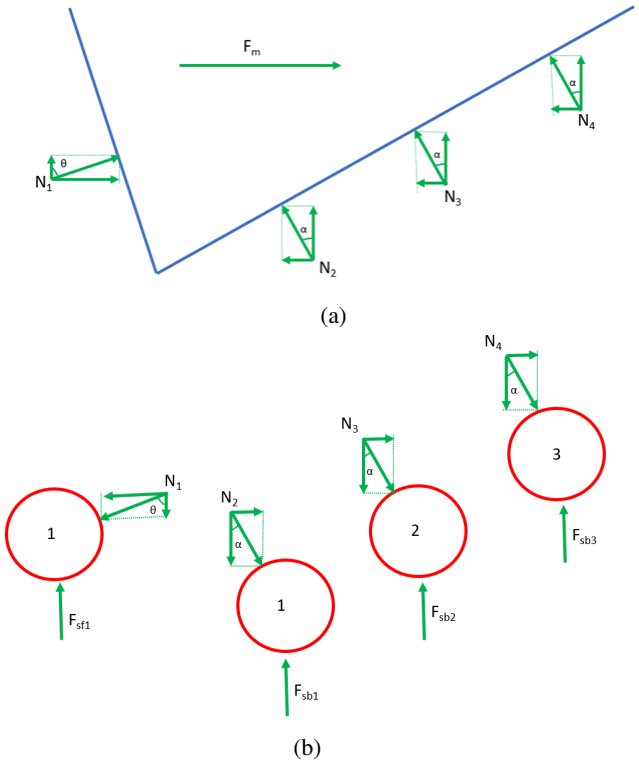

Fig. 25: a. FBD of cam b. FBD of slider

For the equilibrium, the net force in the vertical direction should be zero which gives,

$$F_{sf1} = N_1 \times cos\theta.\ N_1 = F_{sf1} \div cos\theta$$

$$F_{sb1} = N_2 \times cos\alpha.\ N_2 = F_{sb1} \div cos\alpha$$

$$F_{sb2} = N_3 \times cos\alpha.\ N_3 = F_{sb2} \div cos\alpha$$

$$F_{sb3} = N_4 \times cos\alpha.\ N_4 = F_{sb3} \div cos\alpha$$

The net force in the horizontal direction should also be zero which gives,

$$N_1 \times sin\theta + F_m = N_2 \times sin\alpha + N_3 \times sin\alpha + N_4 \times sin\alpha$$

Substituting the spring force in terms of normal reaction,

$$F_m + F_{sf1} \times tan\theta = F_{sb1} \times tan\alpha + F_{sb2}tan\alpha + F_{sb3}tan\alpha$$

$$F_m = F_{sb1} \times tan\alpha + F_{sb2} \times tan\alpha + F_{sb3} \times tan\alpha - (F_{sf1} \times tan\theta)$$

Extrapolating the above equation for n number of advancing and retracting sliders,

$$F_m = (F_{sb1}tan\alpha + F_{sb2}tan\alpha + F_{sb3}tan\alpha + ...F_{sbn}tan\alpha) - (F_{sf1}tan\theta + F_{sf2}tan\theta + F_{sf3}tan\theta + ...F_{sfn}tan\theta)$$

Similar procedure can be followed to calculate the force required by the motor when there is not support from the spring.

$$F_m = F_{sb1}tan\alpha + F_{sb2}tan\alpha + F_{sb3}tan\alpha + ...F_{sbn}tan\alpha$$

APPENDIX C
MOTOR TORQUE CALCULATION

The motor torque was calculated for the 3-jump cam as follows. Since there are 3 backward/forward slopes, there would be a total of 9 retracting sliders/springs.

Initial compression length (l_{ic}) = 5 mm

Compression length at the end of stoke (l_{ec}) = 15 mm

stiffness of the spring (st_s) = 0.06 N/mm

Force in the spring when they are initially compressed (f_{ic}) = l_{ic} × st_s = 0.3 N

Force in the spring when they are compressed to the stroke length of the slider (f_{ec}) = l_{ec} × st_s = 0.9 N

The average force in the spring (F_{savg}) = (f_{ec} + f_{ic}) ÷ 2 = 0.6 N

The force acting on the cam is given by,

$$F_c = F_{s1}tan\alpha + F_{s2}tan\alpha + F_{s3}tan\alpha + F_{s4}tan\alpha + F_{s5}tan\alpha + F_{s6}tan\alpha + F_{s7}tan\alpha + F_{s8}tan\alpha + F_{s9}tan\alpha$$

Where, F_{s1}, F_{s2}, F_{s3}, F_{s4}, F_{s5}, F_{s6}, F_{s7}, F_{s8}, F_{s9} – Force in the springs corresponding to the nine retracting sliders

α – Backward slope of the cam

Since the spring force are same the above equation can be simplified as,

F_c = $9 \times tan\alpha \times F_{savg}$

For 3 jump cam, α = 46°. thus on calculating, F_c = 5.59 N

The above net cam force has to be provided by the motor in the form of torque. Thus, the torque required by the motor is given by,

$$T_m = F_c * R_2$$

Where, R2 is the minimum distance between the centre of the motor shaft to the distal part of the cam profile which is equal to 7 mm.

T_m= 5.59 * 7 = 39.14 N mm

APPENDIX D
DESIGN DRAWINGS

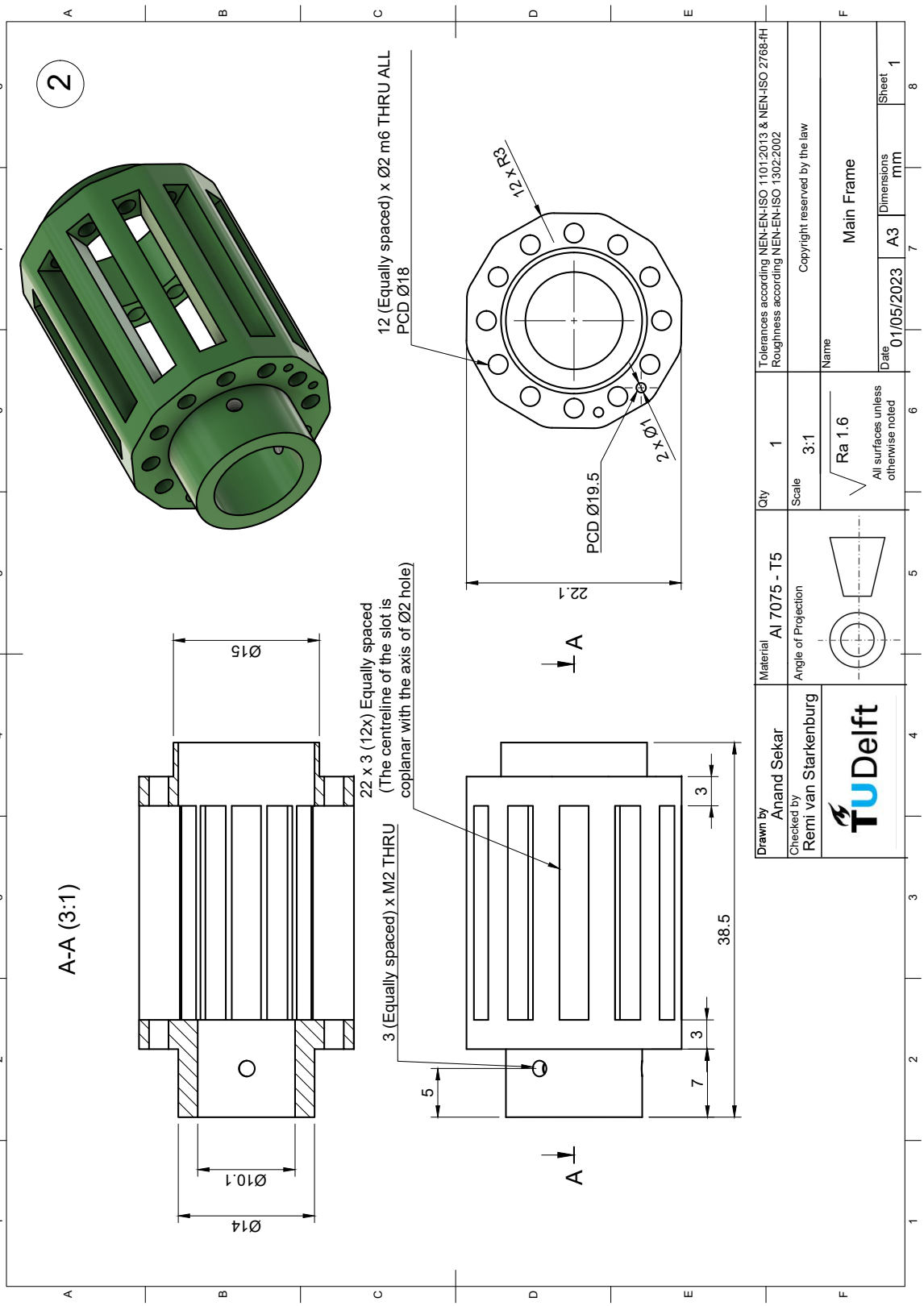
2
12 (Equally spaced) x Ø2 m6 THRU ALL
PCD Ø18
12 x R3
2 x Ø1
PCD Ø19.5
22.1
A
A
A-A (3:1)
Ø15
Ø10.1
Ø14
22 x 3 (12x) Equally spaced
(The centreline of the slot is
coplanar with the axis of Ø2 hole)
3 (Equally spaced) x M2 THRU
3
3
38.5
7
5
Drawn by
Anand Sekar
Checked by
Remi van Starkenburg
Material
Al 7075 - T5
Angle of Projection
Qty
1
Scale
3:1
Ra 1.6
All surfaces unless
otherwise noted
Tolerances according NEN-EN-ISO 1101:2013 & NEN-ISO 2768-fH
Roughness according NEN-EN-ISO 1302:2002
Copyright reserved by the law
Name
Main Frame
Date
01/05/2023
A3
Dimensions
mm
Sheet
1
TUDelft

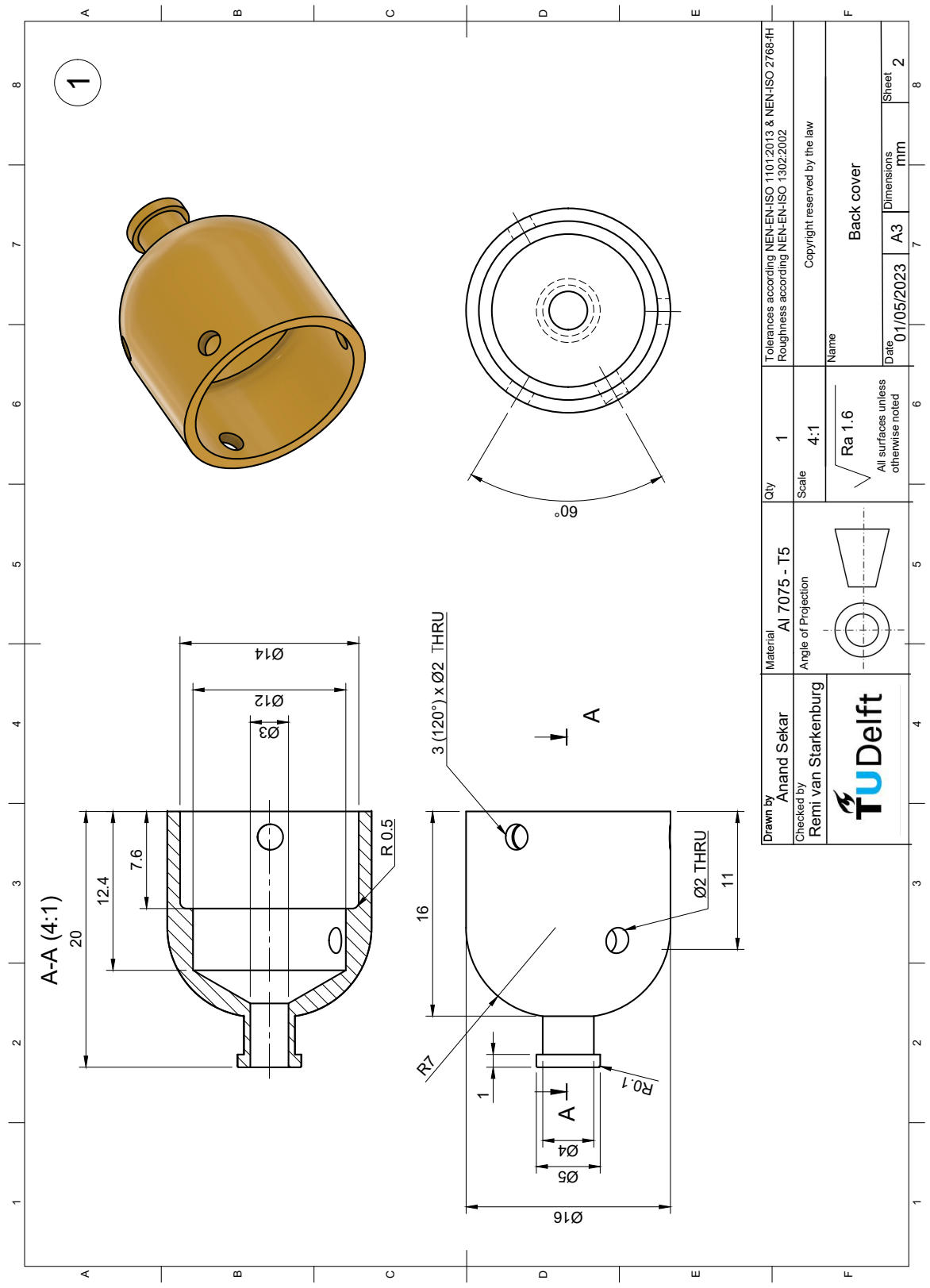
1
60°
A-A (4:1)
20
12.4
7.6
Ø14
Ø12
Ø3
R 0.5
3 (120°) x Ø2 THRU
A
16
Ø2 THRU
11
R7
1
R0.1
Ø4
Ø5
Ø16
Drawn by
Anand Sekar
Checked by
Remi van Starkenburg
TUDelft
Material
Al 7075 - T5
Angle of Projection
Qty
1
Scale
4:1
Ra 1.6
All surfaces unless otherwise noted
Tolerances according NEN-EN-ISO 1101:2013 & NEN-ISO 2768-fH
Roughness according NEN-EN-ISO 1302:2002
Copyright reserved by the law
Name
Back cover
Date
01/05/2023
A3
Dimensions
mm
Sheet
2

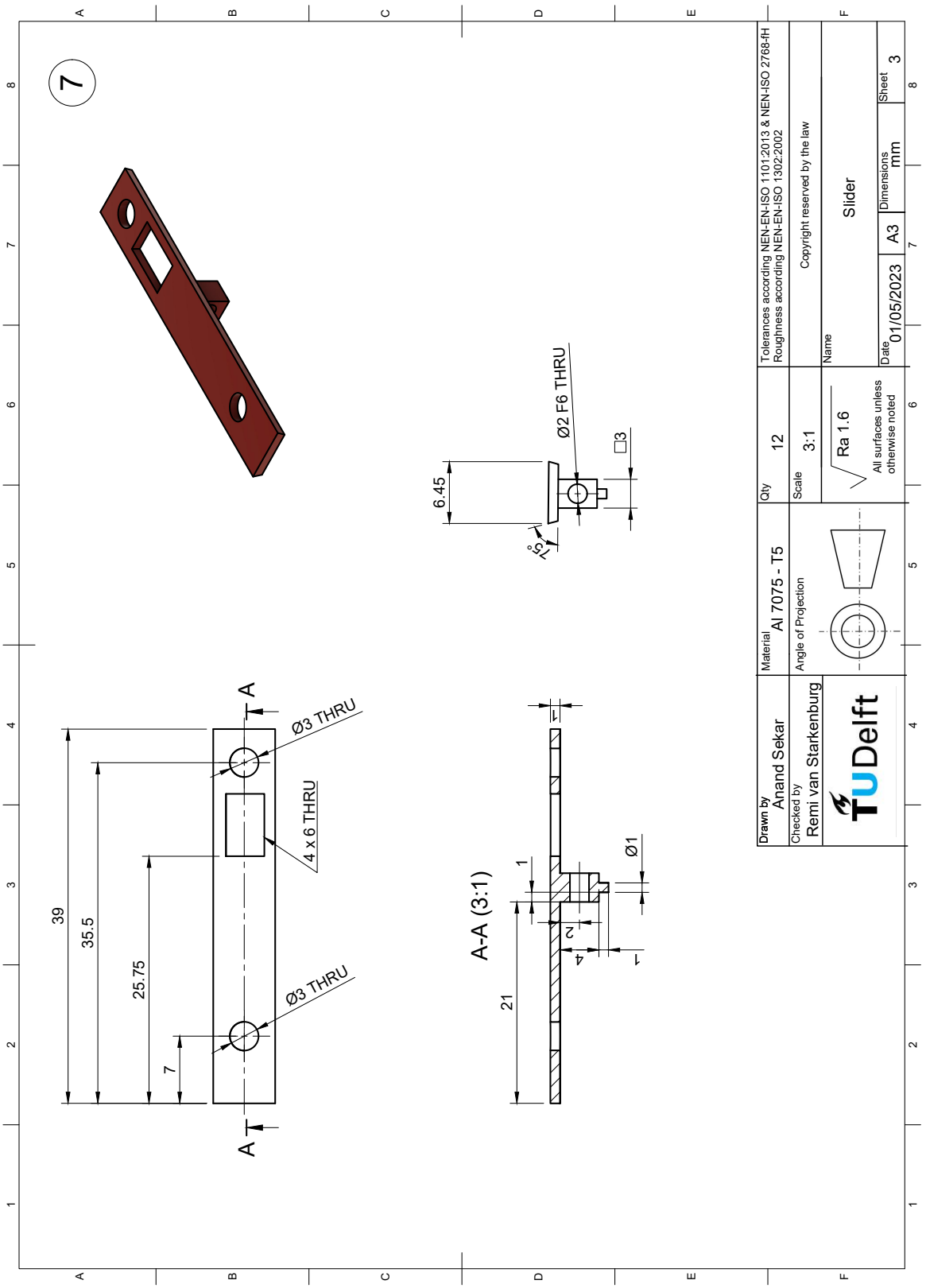
7
Ø3 THRU
4 x 6 THRU
Ø3 THRU
39
35.5
25.75
7
A
A
A-A (3:1)
21
1
2
4
1
Ø1
6.45
Ø2 F6 THRU
□3
45°
Drawn by
Anand Sekar
Checked by
Remi van Starkenburg
TUDelft
Material
Al 7075 - T5
Angle of Projection
Qty
12
Scale
3:1
Ra 1.6
All surfaces unless otherwise noted
Tolerances according NEN-EN-ISO 1101:2013 & NEN-ISO 2768-fH
Roughness according NEN-EN-ISO 1302:2002
Copyright reserved by the law
Name
Slider
Date
01/05/2023
A3
Dimensions
mm
Sheet
3

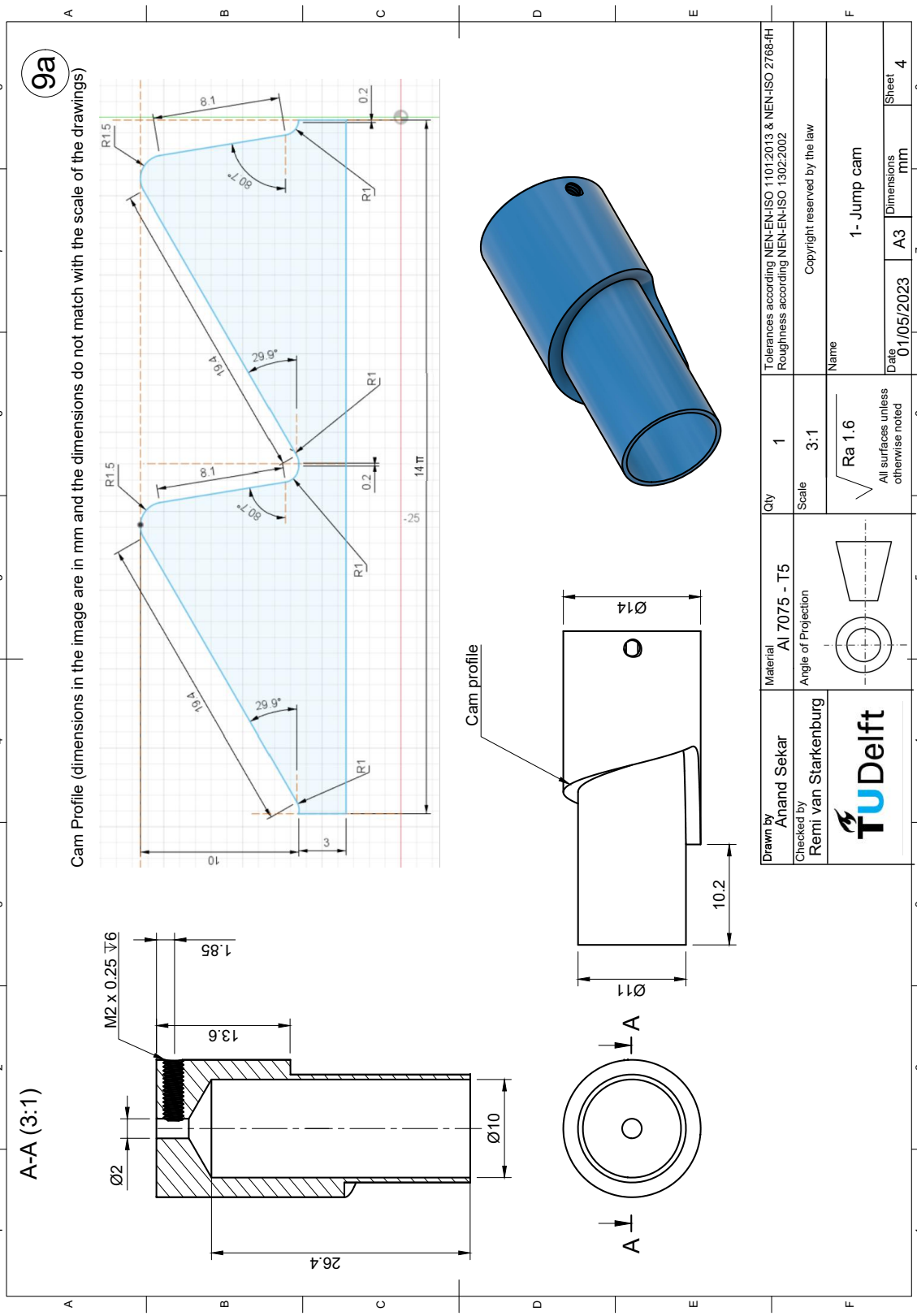
9a
Cam Profile (dimensions in the image are in mm and the dimensions do not match with the scale of the drawings)
A-A (3:1)
Cam profile
M2 x 0.25 ↧6
1.85
13.6
Ø2
Ø10
26.4
Ø14
Ø11
10.2
Drawn by Anand Sekar
Checked by Remi van Starkenburg
Material Al 7075 - T5
Angle of Projection
Qty 1
Scale 3:1
Ra 1.6
All surfaces unless otherwise noted
Tolerances according NEN-EN-ISO 1101:2013 & NEN-ISO 2768-fH
Roughness according NEN-EN-ISO 1302:2002
Copyright reserved by the law
Name 1- Jump cam
Date 01/05/2023
A3
Dimensions mm
Sheet 4
TU Delft

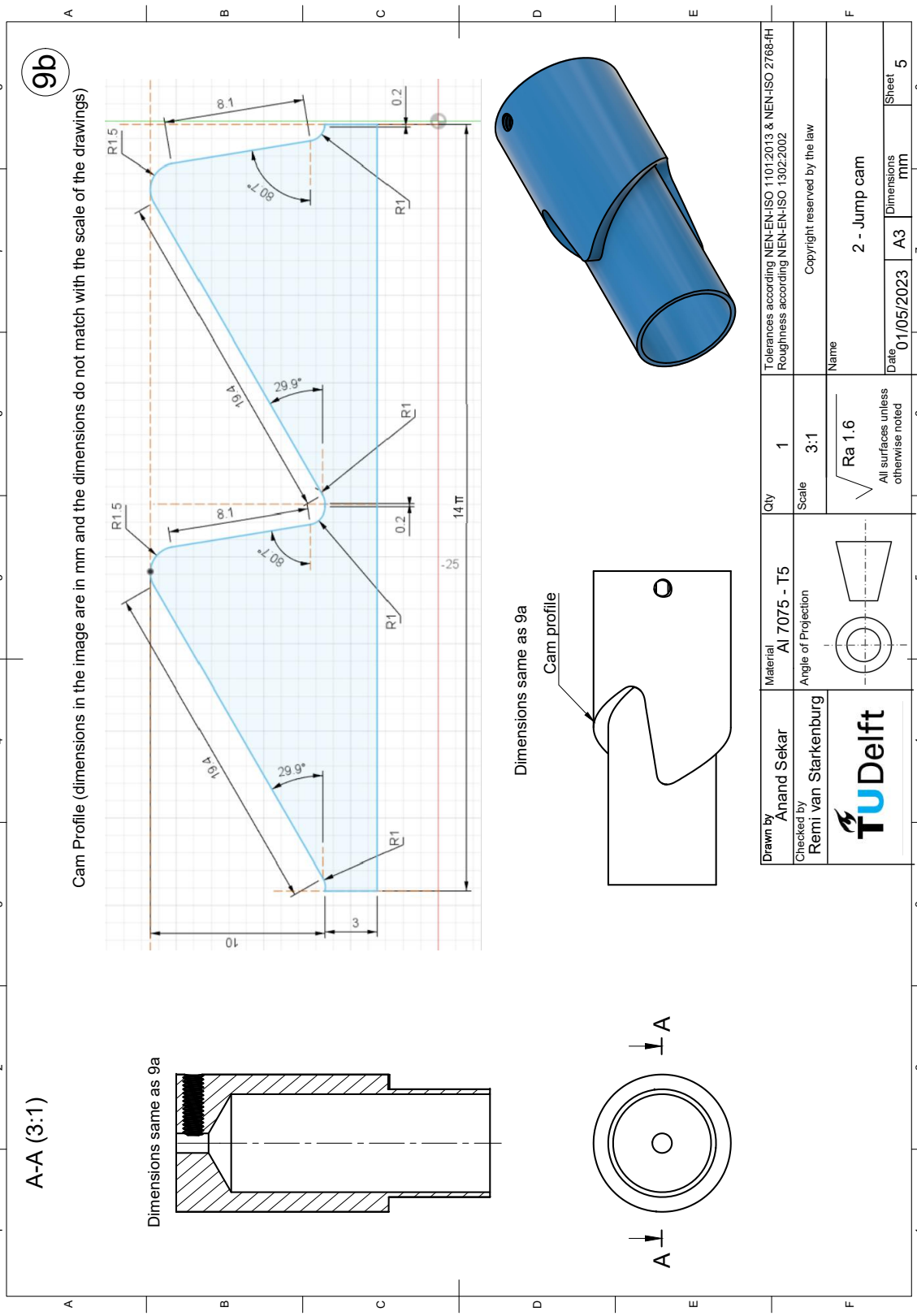
9b
Cam Profile (dimensions in the image are in mm and the dimensions do not match with the scale of the drawings)
A-A (3:1)
Dimensions same as 9a
Dimensions same as 9a
Cam profile
Drawn by Anand Sekar
Checked by Remi van Starkenburg
Material Al 7075 - T5
Angle of Projection
Qty 1
Scale 3:1
Ra 1.6
All surfaces unless otherwise noted
Tolerances according NEN-EN-ISO 1101:2013 & NEN-ISO 2768-fH
Roughness according NEN-EN-ISO 1302:2002
Copyright reserved by the law
Name 2 - Jump cam
Date 01/05/2023
A3
Dimensions mm
Sheet 5
TU Delft

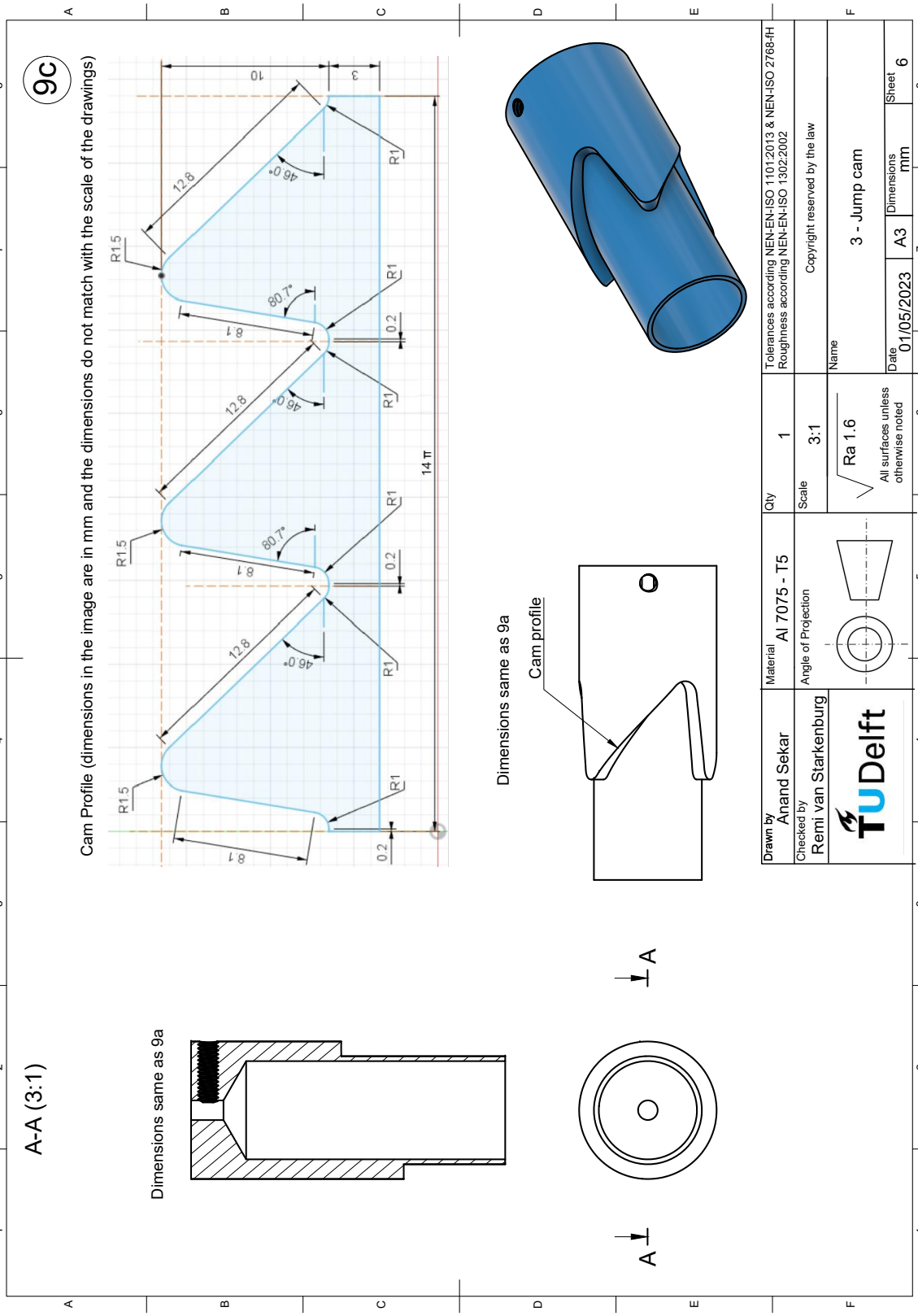
9c
A-A (3:1)
Cam Profile (dimensions in the image are in mm and the dimensions do not match with the scale of the drawings)
Dimensions same as 9a
Cam profile
Dimensions same as 9a
A
A
Drawn by Anand Sekar
Checked by Remi van Starkenburg
Material Al 7075 - T5
Angle of Projection
Qty 1
Scale 3:1
Ra 1.6
All surfaces unless otherwise noted
Tolerances according NEN-EN-ISO 1101:2013 & NEN-ISO 2768-fH
Roughness according NEN-EN-ISO 1302:2002
Copyright reserved by the law
Name 3 - Jump cam
Date 01/05/2023
A3
Dimensions mm
Sheet 6
TU Delft

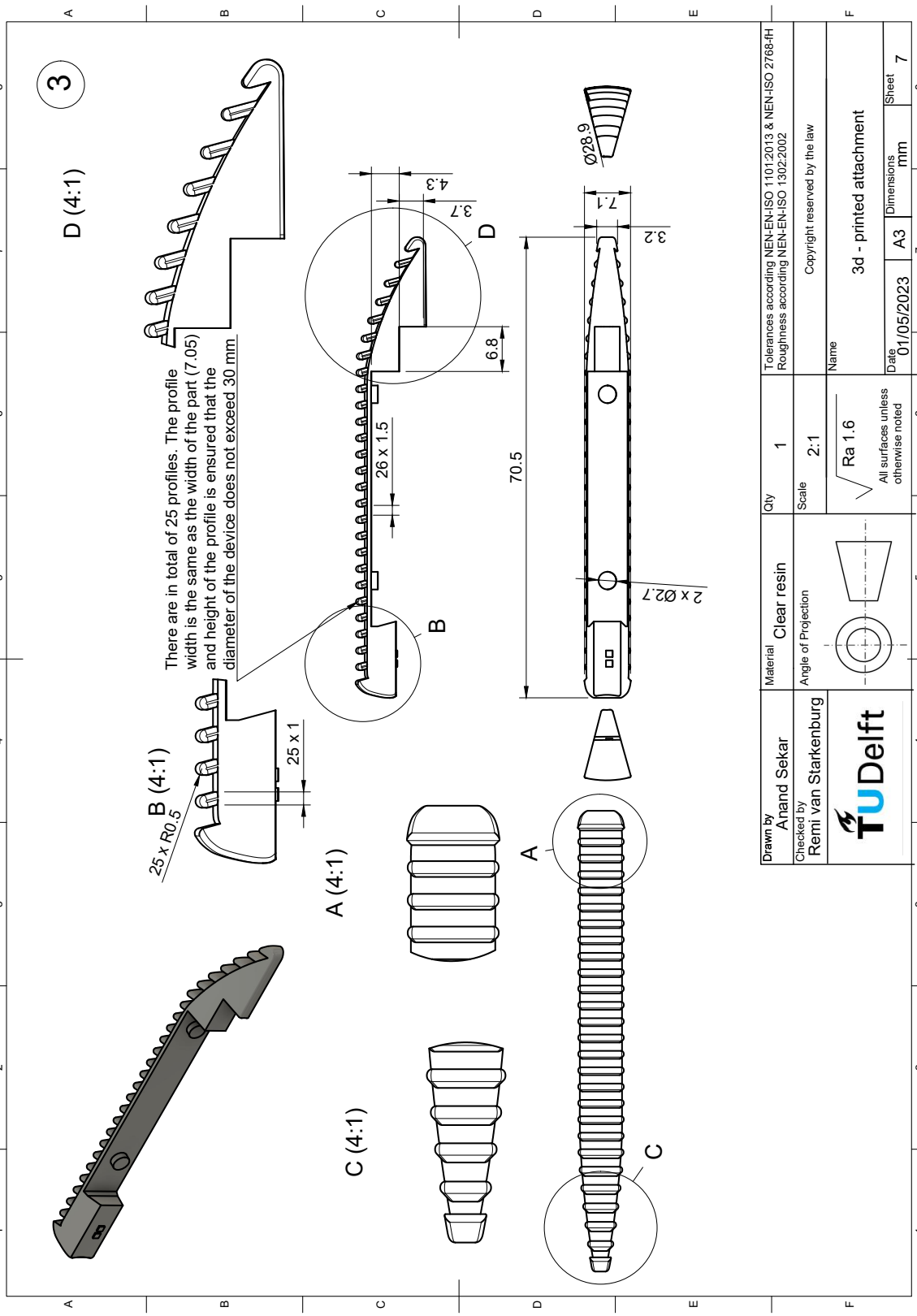
3
D (4:1)
There are in total of 25 profiles. The profile width is the same as the width of the part (7.05) and height of the profile is ensured that the diameter of the device does not exceed 30 mm
B (4:1)
25 x R0.5
25 x 1
A (4:1)
C (4:1)
26 x 1.5
4.3
3.7
6.8
D
B
A
C
70.5
Ø28.9
7.1
3.2
2 x Ø2.7
Drawn by Anand Sekar
Checked by Remi van Starkenburg
TUDelft
Material Clear resin
Angle of Projection
Qty 1
Scale 2:1
Ra 1.6
All surfaces unless otherwise noted
Tolerances according NEN-EN-ISO 1101:2013 & NEN-ISO 2768-fH
Roughness according NEN-EN-ISO 1302:2002
Copyright reserved by the law
Name
3d - printed attachment
Date 01/05/2023
A3
Dimensions mm
Sheet 7

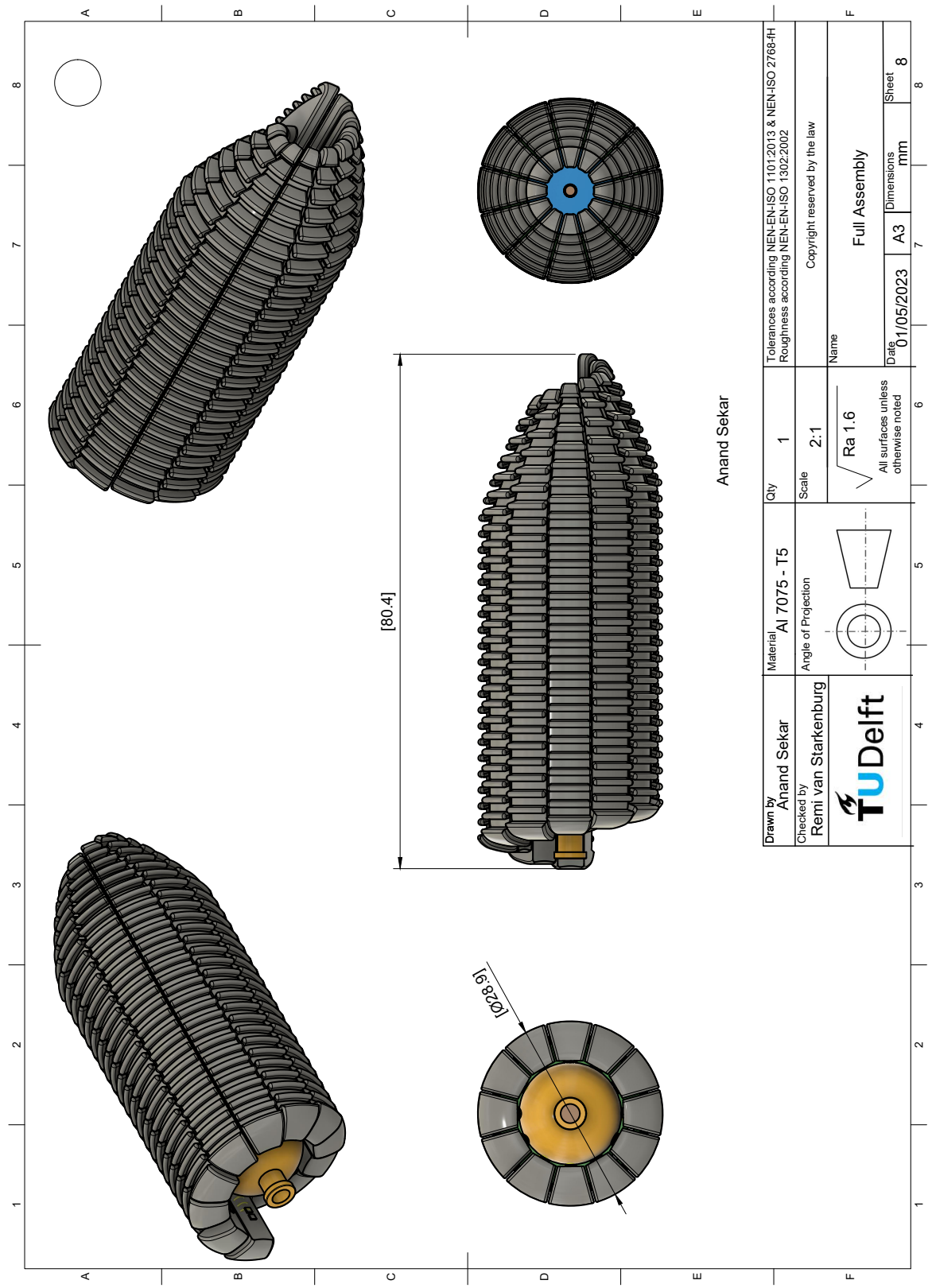
[80.4]
[Ø28.91]
Anand Sekar
Drawn by
Anand Sekar
Checked by
Remi van Starkenburg
Material
Al 7075 - T5
Angle of Projection
Qty
1
Scale
2:1
Ra 1.6
All surfaces unless otherwise noted
TUDelft
Tolerances according NEN-EN-ISO 1101:2013 & NEN-ISO 2768-fH
Roughness according NEN-EN-ISO 1302:2002
Copyright reserved by the law
Name
Full Assembly
Date
01/05/2023
A3
Dimensions
mm
Sheet
8

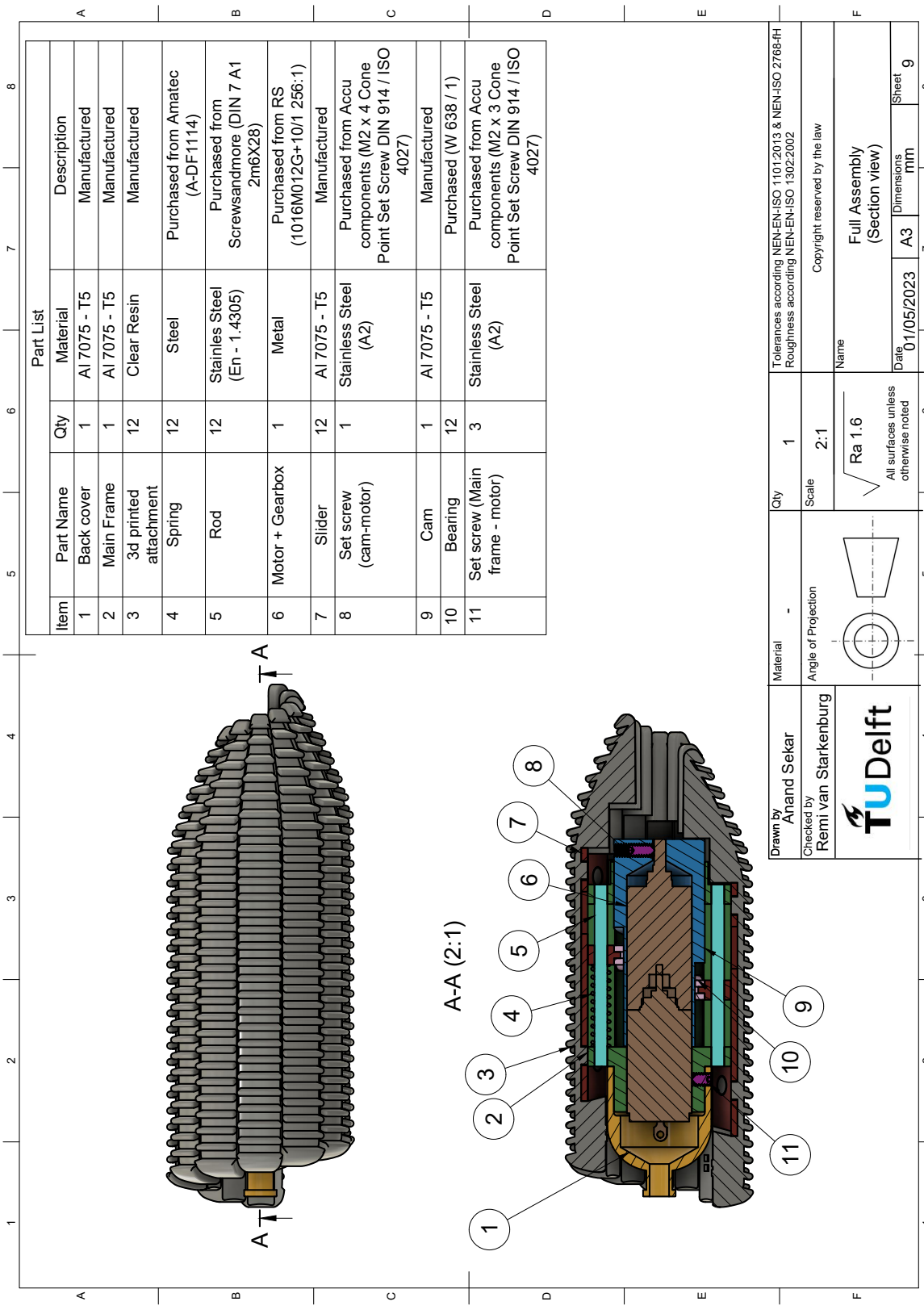
Part List
Item | Part Name | Qty | Material | Description
1 | Back cover | 1 | Al 7075 - T5 | Manufactured
2 | Main Frame | 1 | Al 7075 - T5 | Manufactured
3 | 3d printed attachment | 12 | Clear Resin | Manufactured
4 | Spring | 12 | Steel | Purchased from Amatec (A-DF1114)
5 | Rod | 12 | Stainles Steel (En - 1.4305) | Purchased from Screwsandmore (DIN 7 A1 2m6X28)
6 | Motor + Gearbox | 1 | Metal | Purchased from RS (1016M012G+10/1 256:1)
7 | Slider | 12 | Al 7075 - T5 | Manufactured
8 | Set screw (cam-motor) | 1 | Stainless Steel (A2) | Purchased from Accu components (M2 x 4 Cone Point Set Screw DIN 914 / ISO 4027)
9 | Cam | 1 | Al 7075 - T5 | Manufactured
10 | Bearing | 12 | | Purchased (W 638 / 1)
11 | Set screw (Main frame - motor) | 3 | Stainless Steel (A2) | Purchased from Accu components (M2 x 3 Cone Point Set Screw DIN 914 / ISO 4027)
A
A
A-A (2:1)
1
2
3
4
5
6
7
8
9
10
11
Drawn by Anand Sekar
Checked by Remi van Starkenburg
Material -
Angle of Projection
Qty 1
Scale 2:1
Ra 1.6
All surfaces unless otherwise noted
Tolerances according NEN-EN-ISO 1101:2013 & NEN-ISO 2768-fH
Roughness according NEN-EN-ISO 1302:2002
Copyright reserved by the law
Name
Full Assembly (Section view)
Date 01/05/2023
A3
Dimensions mm
Sheet 9
TU Delft